Decoupling of degradation from deadenylation reshapes poly(A) tail length in yeast meiosis

Decoupling of degradation from deadenylation reshapes poly(A) tail length in yeast meiosis

David Wiener, Yaron Antebi#, Schraga Schwartz#

Department of Molecular Genetics, Weizmann Institute of Science, Rehovot 7610001, Israel

- corresponding authors

Yaron Antebi - ayaron@weizmann.ac.il
Schraga Schwartz - schwartz@weizmann.ac.il

Abstract

Nascent mRNA is endowed with a poly(A) tail, which is subject to gradual deadenylation in the cytoplasm, followed by mRNA degradation. Deadenylation and degradation rates are typically correlated, rendering it difficult to dissect the individual determinants governing each of these processes. In addition, the mechanistic basis for the coupling between deadenylation and degradation and the extent to which the two can be decoupled are largely unknown. Here we developed an approach allowing systematic, robust and multiplexed quantification of poly(A) tails. Our results suggest that in yeast, exclusively during meiosis, mRNA deadenylation and degradation rates are decoupled. The decoupled regime in meiosis allowed us to discover transcript length as a major determinant of deadenylation rates and as a key contributor to the reshaping of poly(A) tail lengths in meiosis. The meiosis-specific decoupling also led to unique positive associations between poly(A) tail length and gene expression. The decoupling of degradation from deadenylation is also strongly associated with a focal localization pattern of the RNA degradation factor Xrn1 and can be phenocopied by deletion of Xrn1 under non-meiotic conditions. Importantly, the association of transcript length with deadenylation rates is conserved across eukaryotes. This study uncovers a new factor that shapes deadenylation rate and discovers a unique context in which degradation is decoupled from deadenylation.

Introduction

The non-templated addition of adenosines to the 3' ends of most eukaryotic mRNA, forming a poly(A) tail, is a highly conserved process throughout all eukaryotes. Poly(A) tails are formed in the nucleus by poly(A) polymerases (PAPs), which add up to 250 adenosines to mammalian transcripts and up to 90 in yeast [1]. Following export into the cytoplasm, poly(A) tails undergo progressive deadenylation, whereby the bulk deadenylation activity in yeast is mediated via two exonucleases, Ccr4 and Pop2 [2]. Once the length of the poly(A) tail is reduced beyond a certain threshold of 20-25 nt [3–5], the short-tailed transcripts are subjected to decapping and subsequent 5'-3' degradation via Xrn1 [6,7]. The poly(A) tail thus plays a major role in the regulation of mRNA stability [8].

Poly(A) tail lengths distribution is determined by three processes: synthesis, deadenylation and degradation [9]. While most transcripts are formed with similar tail lengths, deadenylation rates and degradation rates have a broad (1000-fold each) range [9,10]. Diverse mechanisms are known to play a role in recruiting the deadenylase machinery towards individual genes, such as RNA binding proteins [11–13], RNA methylation [14] and microRNAs [15,16]. However, whether there are *global* determinants impacting these rates, and whether such determinants can vary between different conditions is largely unknown. To date, there exist only few examples in which concerted, temporally coherent changes in poly(A) tail lengths have been observed on the basis of transcriptome-wide measurements. These include the observations of coordinated tail length changes during oocyte-to-embryo development [17,18], and timely controlled deadenylation, which is critical for proper circadian cycles [19,20]. Such global reshaping of poly(A) tail lengths raises the question of whether and how they can arise from changes in synthesis, deadenylation and/or degradation. Importantly, works perturbing the deadenylation and degradation machineries have shown an impact in poly(A) tai length distributions [21–23].Recently, a study inferring transcriptome-wide production, deadenylation and degradation rates uncovered that in mammalian cell lines deadenylation rates are correlated with degradation rates [9]. What drives this coupling, how generalizable it is and whether this coupling can be lost under particular conditions remains to be explored.

In the budding yeast, *Saccharomyces cerevisiae*, diploid yeast starved for nitrogen and fermentable carbon sources trigger a complex program coupling meiosis with spore formation [24]. Yeast meiosis represents an attractive model to study poly(A) tail regulation for several reasons. First, it is a process coupling extensive transcriptional and post-transcriptional regulation, including coordinated and pervasive changes in gene expression and translation [25,26], extensive transcription of non-coding RNAs [27], unique activation of RNA methylation pathway [28,29] and transcript isoform switching [26], leading us to hypothesize that poly(A)-tails might be subjected to regulation as well. Second, yeast also offers unique advantages in terms of the well-characterized deadenylation and degradation machinery components, most of which are present in only a single paralog (in contrast to mammalian systems harboring more redundancy), its genetic tractability, and the fact that poly(A) tails in yeast are substantially shorter than in mammalian species, reducing the technical barriers in accurately measuring them [30].

Technical limitations in quantifying the length of the poly(A) tail has limited our knowledge pertaining to poly(A) tail regulation. Illumina-based sequencing technologies have been limited in their ability to adequately read through homopolymers, only allowing quantification of homopolymers up to ~30 bp long. This limitation was overcome, in one case (TAIL-seq), through reanalysis of raw sequencing cluster images from which tail-length was inferred [31], and in another case (PAL-seq) using a complex technical setup, performed directly on the flowcells of the sequencing machines, quantitatively labelling each sequencing cluster with biotin in proportion to the length of the poly(A) tail. However, both approaches rely on now outdated sequencing platforms [17,30]. In recent years, protocols based on Pacbio sequencing were developed [32,33]; However, these approaches are limited by the sequencing depth that one can realistically obtain using this platform, as by the general unavailability of this platform and its technical limitations. In addition, all three available approaches require relatively high amounts of

starting material and provide readouts for only a single sample at the time, limiting their scalability, increasing both the cost per experiment and the technical variability due to sample-specific processing steps.

Here we develop a multiplexed approach for measuring poly(A) tail lengths and generate poly(A) tail maps across a dense time course preceding and throughout yeast meiosis. We find that the poly(A) tail lengths are dynamically reshaped along the meiotic time course. Remarkably, we found that a major determinant associated with poly(A) tail length exclusively during meiosis - but not during vegetative growth conditions - is transcript length. By combining modeling with perturbational approaches, we converge on two key findings. First, that transcript length is tightly inversely associated with deadenylation rates both under meiotic and mitotic conditions. Second, that deadenylation and degradation are decoupled during meiosis, resulting in accumulation of deadenylated, but not degraded, mRNAs. Mechanistically, we demonstrate that the decoupling of degradation from deadenylation is associated with relocalization of Xrn1 into distinct foci, upon onset of meiosis. Finally, we demonstrate that the association between transcript length and deadenylation rate is conserved also in mammals. Our study highlights a novel determinant of mRNA deadenylation, and demonstrates how decoupling of deadenylation from degradation can lead to reshaping of poly(A) tail profiles and of gene expression over the course of a biological response.

Results

Development of a multiplexed approach for quantifying poly(A) tail length

To allow robust, cost-efficient and multiplexed profiling of poly(A) tails, we developed multiplexed poly(A) tail sequencing (mPAT-seq). This new protocol is inspired by TAIL-seq [31], but with two important adaptations. First, it does not require now-obsolete sequencing platforms, but rather is compatible with NextSeq and NovaSeq Illumina platforms. Second, it relies on barcoding of samples at a very early step, which allows processing up to a dozen samples in a single test-tube (this number can in principle be expanded further). This multiplexing considerably reduces cost, labor and likely also the technical variability associated with the measurements. In addition, such multiplexing dramatically reduces the required amount of input material: mPAT-seq requires only 400 ng of total RNA per sample, compared to 100 µg required by TAIL-seq, 5-25 µg required by PAL-Seq v2[9] or 1-5 µg required by mTAIL-seq [17]. mPAT-seq consists of the following steps: (1) ligation of a barcoded adapter to the 3' end of RNAs of up to 12 samples, (2) pooling of the samples, (3) rRNA depletion, (4) partial RNA fragmentation with RNaseT1 which only cleaves after guanine thereby leaving the poly(A) tail intact, (5) reverse transcription, primed on the adapter ligated in step 1, (6) ligation of a second adapter to the 3' end of the cDNA, (7) PCR amplification and sequencing **(Fig. 1A)**. The libraries are sequenced from both ends, whereby a short read (e.g. ~40 bp) from the 5' end is sufficient for providing the identity of the transcript and a long read (~110 bp) from the 3' end allows quantifying the length of the poly(A) tail. For data analysis, we generated a computational pipeline handling the demultiplexing, alignment, QC, and poly(A) tail quantification of each set of reads, and culminating with a *distribution* of all tail lengths associated with each gene in a given sample.

A major concern was that the poly(A) homopolymer might not be adequately sequenced. In the past, the inability to sequence through homopolymeric runs was the key motivation to develop a computational framework reanalyzing raw images generated by now-outdated sequencing platforms from which poly(A) tail length was then inferred [31]. To evaluate the ability of different sequencing platforms to adequately sequence through poly(A) homopolymers of defined identity, we synthesized a series of DNA spike-ins with tails ranging from 11-76 nt. We found that both NovaSeq and NextSeq platforms could accurately quantify the length of these tails (~80% of the reads are within a range of 10% around the expected value and ~95% within 20%) throughout this entire range of tested lengths **(Fig. 1B, Fig. S1A-top)**. Interestingly, this was not the case for MiSeq **(Fig. S1A-bottom)**, which was

only accurate up to ~30nt. The lengths of poly(A) tails in yeast (generally between 10 to 75nt) are thus well within the range of this approach.

We further confirmed that the extent of concurrence between poly(A)-tail measurements across two biological replicates was high (ρ~0.8) when demanding at least 30 reads/transcript, and could be increased even further (up to ρ~0.9) with more stringent demands on the sequencing depth **(Fig. S1B)**. As an additional positive control we measured poly(A) tails in strains lacking the deadenylases Ccr4 and Pop2. Consistent with our expectations, we found the transcript tails in these samples were longer, on average, by 30% in ccr4Δ/Δ and ~10% in pop2Δ/Δ, in a highly significant manner ($P<0.0001$) **(Fig. S1C).**

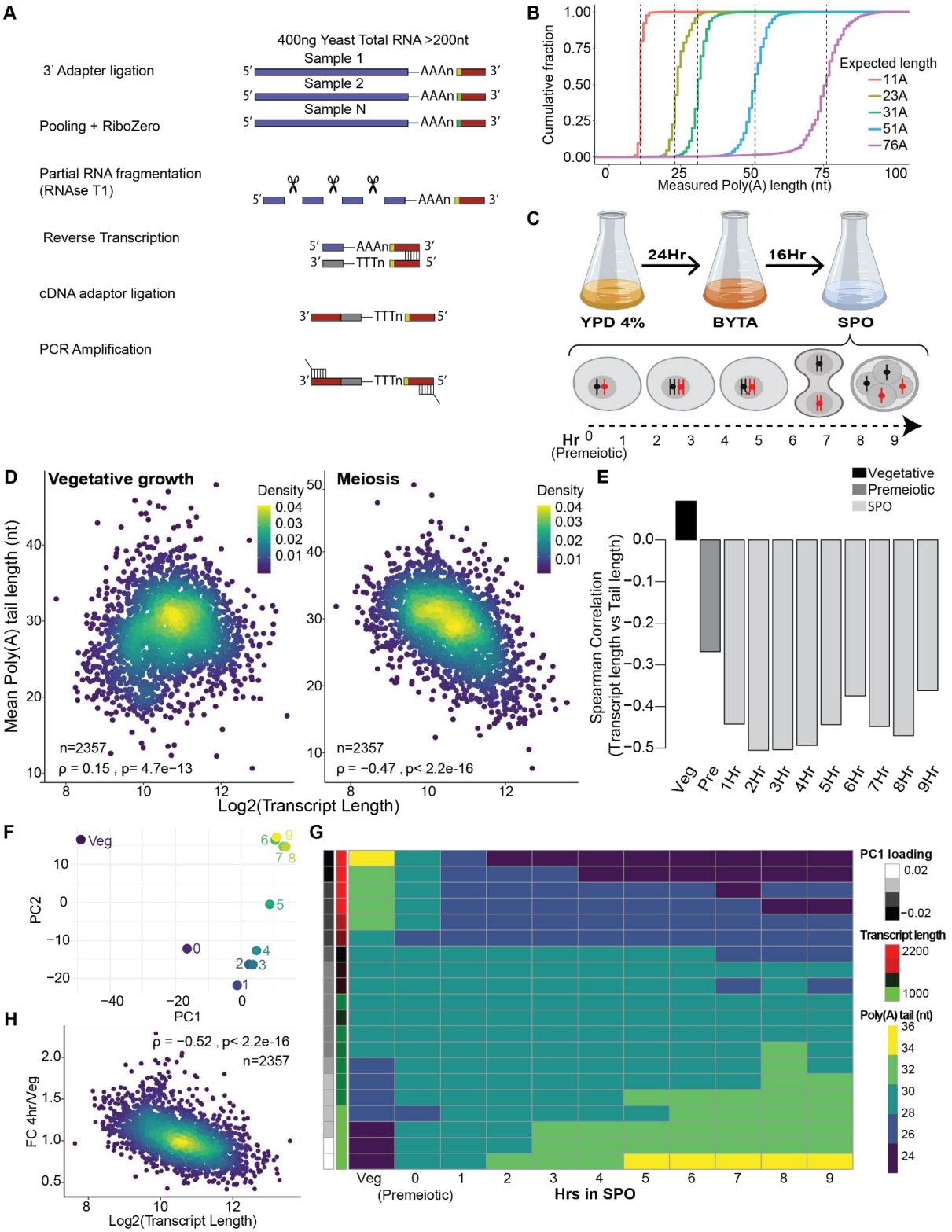

Figure 1. Poly(A) tail reshaping in meiosis is associated with transcript length. A) Schematic view of the multiplexed poly(A) tail sequencing (mPAT-seq) protocol. **B)** Cumulative fraction plot showing quantification of the spike-ins adenosines homopolymeric region length in the NovaSeq platform. Dashed lines are drawn at expected lengths (11,23,31,51,76). **C)** Representation of the meiosis induction protocol and meiotic progression. **D)** Scatterplot of the mean poly(A) tail (nt) vs the log2 of transcript length per gene, both in vegetative growth (left) and after 4 hrs in SPO (right), color code corresponds to the kernel density estimation calculated with the MASS R package [34]. Spearman correlation and the number of genes are presented. **E)** Barplot of Spearman correlation between gene mean poly(A) tail length and log2 of transcript length across the meiosis time course. **F)** Principal component analysis using scaled poly(A) tail length measurements indicates that poly(A) tail profiles progress with

meiosis. Color code corresponds to meiotic progression.**G)** Genes were sorted by PC1 loadings and aggregated in 20 groups. The mean poly(A) tail length of each group across the meiotic time course is represented in the heatmap. Additional columns with the mean transcript length (green to red) and PC1 loadings (black to white) of each group were added. **H)** Scatterplot of the mean poly(A) tail fold change per gene between the 4hrs timepoint and the vegetative growth state vs the log2 of transcript length.Figure was generated like D.

Poly(A) tails are progressively reshaped during meiosis to increase anticorrelation with transcript length

We next applied mPAT-seq to RNA extracted from a densely sampled meiotic time course **(Fig. 1C).** This time course encompasses cells monitored under vegetative conditions (Veg), cells grown in nutrient limited BYTA media preparing them for synchronous entry into meiosis (pre-meiotic), and hourly timepoints from 1 to 9 hours following the induction of meiosis. The synchronic progression of meiosis, including DNA replication during the first 4-5 hours, meiosis I and II (5-8 hours) and final spore formation at 24 hours were confirmed by FACS **(Fig. S2A),** nuclear staining **(Fig. S2B)**,and spore counting **(Fig. S2C)**.

In the context of an exploratory analysis aiming to understand the determinants of heterogeneity in tail lengths between genes and across conditions, we noted that the onset of meiosis gave rise to an association between poly(A) tail length and transcript length ('transcript-tail correlation'). In cells growing under vegetative growth conditions, a weak positive correlation between poly(A) tail length and transcript length is observed (ρ=0.15). Premeiotic cells (0 hr timepoint), immediately after BYTA incubation, presented a low negative correlation (ρ=-0.27). Already 1 hr following transfer into SPO medium, the correlation became increasingly negative (ρ=-0.45) and remained at a similar magnitude across the entire time course **(Fig. 1D-E)**.

We next sought to understand whether the emergence of this association in meiosis played a role in reshaping poly(A) tails during meiosis. Inspection of mean poly(A) profiles along meiosis revealed major changes in poly(A) tail lengths. This effect is captured well via principal component analysis (PCA), revealing that the first principle component (PC1) (accounting for ~25% of the variability) follows the progression through meiosis **(Fig. 1F)**. Remarkably, PC1 correlated strongly with transcript length (ρ=-0.46), suggesting that ~20% of the variability in PC1 is attributed to transcript length (**Fig. S1D-E).** To visualize this result, we binned all expressed genes into 20 groups (roughly 150 genes / group) based on their PC1 loadings, and plotted the mean tail length for each bin, per each timepoint. This analysis revealed that this principle component is defined by tails undergoing coherent and consistent changes along the progression of meiosis: At its one ("negative") extreme are long genes with long tails (~35 bp on average) under vegetative conditions shortening during meiosis (down to ~24 bp on average), whereas at its other ("positive") extreme are short genes with short tails under vegetative conditions that get extended during meiosis **(Fig. 1G)**. The most dramatic effects were observed in the transition from vegetative growth conditions to growth under glucose deprived media. Consistently, there was a strong correlation (ρ=-0.52) between transcript length and the fold-change in poly(A) tail length between a 4-hr timepoint and the vegetative timepoint **(Fig. 1H)**. Thus, these analyses demonstrate that the entry into meiosis gives rise to a uniquely observed relationship between transcript length and poly(A) tail length, and that this association is a significant force contributing to the reshaping of poly(A) tails during meiosis.

Meiosis can be triggered in yeast via deprivation of nutrient sources. To distinguish whether the association of tail length with transcript length was a consequence of the meiotic-specific cellular program or directly due to lack of nutrient sources, we employed two approaches. **First,** we used a diploid strain incapable of entering meiosis (*MAT*a/a) [35] and subjected it to sporulation medium (SPO). Similar to a meiosis proficient strain, after 3 hr in SPO a negative correlation between poly(A) tail length and transcript length was observed in the meiosis deficient cells (ρ=-0.4) **(Fig. S3A)**, demonstrating that the metabolic conditions are sufficient to induce this relationship. **Second**, we transferred sporulating yeast cells into nutrient-rich media at early (1 hr) and late (7 hr) stages following induction of meiosis

('return-to-growth'(RtG)) **(Fig. S3B)**. Sporulating yeast cells subjected to return-to-growth during *early* stages of meiosis can exit the meiotic program and return to mitotic cell division. However, the return-to-growth capacity is limited because after a certain stage cells are committed to complete sporulation [36]. As expected, cells that were in SPO for only 1hr did not form spores after returning to rich media while cells that stayed in SPO for 7 hr before the transfer were committed to complete the meiotic program **(Fig. S3C)**. Interestingly, in uncommitted cells the transcript–tail-length association decreased after transfer to rich media, whereas in committed cells this correlation was maintained despite the transfer to rich media **(Fig. S3D)**. Consistently, poly(A) tail profiles of committed cells are clustered with meiotic tail profiles while uncommitted cells formed a separated cluster **(Fig. S3E)**. Thus, while nutrient depletion is sufficient for induction of a transcript-tail-length association, it is not essential for its persistence.

Establishing a theoretical model for dissecting determinants governing poly(A) tail lengths

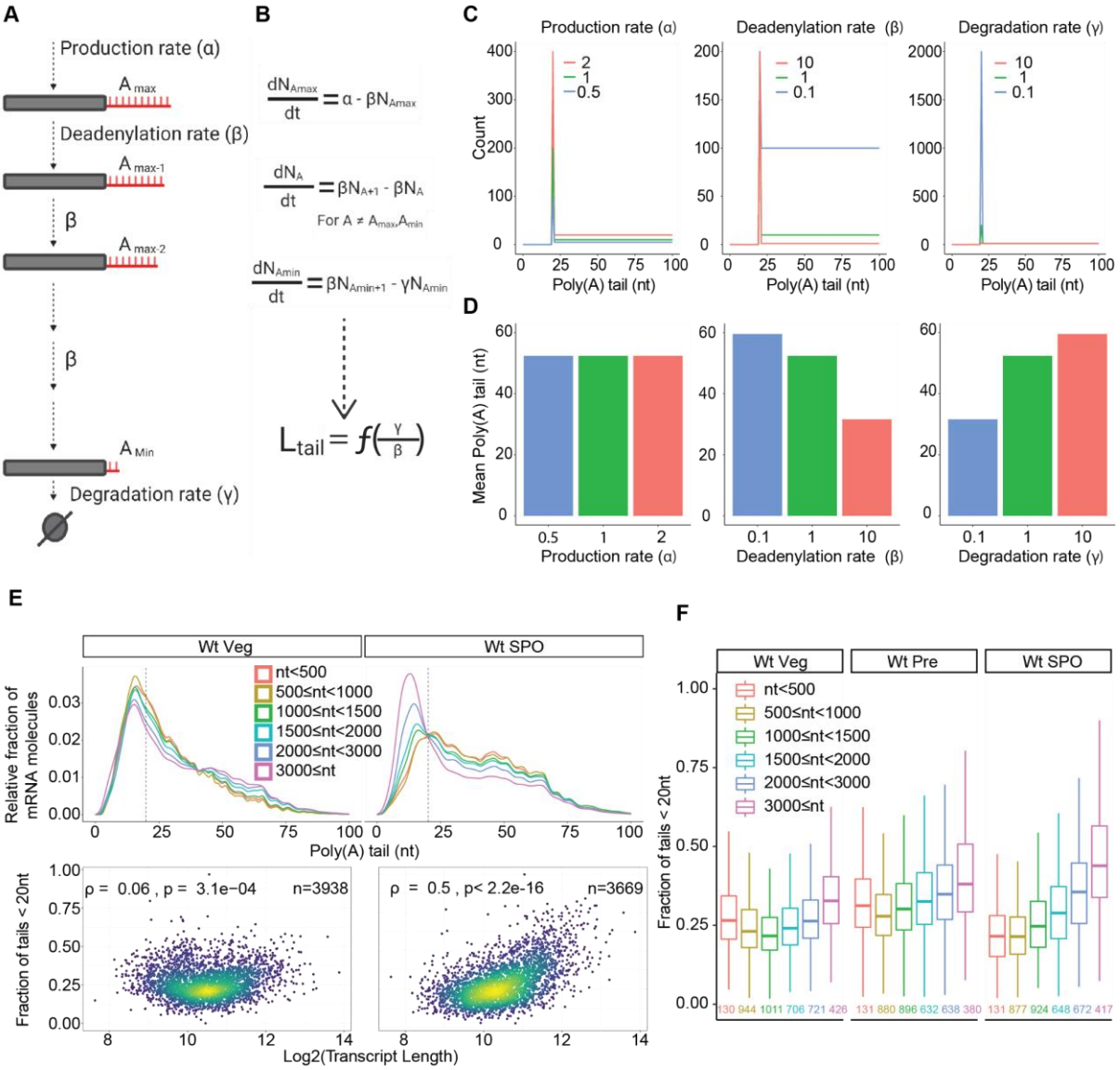

Figure 2. Model for poly(A) tail length dynamics. A) Schematic representation of the 3 steps model of poly(A) tail length regulation. **B)** Set of differential equations that define poly(A) tail distribution (Details in material and methods). **C-D)** Impact of changes in production (Left), deadenylation (Center), degradation (Right) and rates (bottom-left) on poly(A) tail distribution with fixed A_{max}(100nt) and A_{min}(20nt), different rate values are arbitrary units reflecting the relative difference between them. In C a histogram of tail lengths is shown following perturbation of a single parameter. In D mean tail lengths per each perturbation are shown. **E)** Top, Tail length distributions of mRNA molecules in meiosis and vegetative growth, genes were grouped by transcript length and a dashed line

was drawn at 20nt. Bottom, Scatterplot of the short tails fraction vs the log2 of transcript length, both in vegetative growth (left) and after 5 hrs in SPO (right).The figure was generated like in Fig. 1D. .**F)** Boxplot of the fraction of tails under 20nt per genes and plotted by transcript length groups. Number of genes per group is indicated with the corresponding specific color.

To better understand the role of transcript length in shaping poly(A) tails, we first established a theoretical framework quantitatively modelling the formation and elimination of poly(A) tails. Drawing on work performed by the Bartel lab[9], we developed a more simplified model based on the assumption that the poly(A) tail length is shaped in 3 steps.1) Poly(A) tails with a fixed tail length of A_{max} are produced at a rate of α. 2) Poly(A) tails are iteratively deadenylated at a rate of β, down to a length of A_{min}. 3) Deadenylated transcripts of length A_{min} are removed (i.e. decapped and degraded) at a rate of γ. (**Fig. 2A**). Of note, while the essence of the two models is similar, in the previous work which aimed to extract gene-specific parameters, the distribution of production and degradation rates assumed a specific functional form, whereas in our model which primarily aimed to understand the dependency between parameters, we used a more minimal model. Specifically, the two key assumptions of the model are that A_{min} and A_{max} are constant across all genes and that deadenylation rates are not a function of poly(A) tail length. Such a model can be solved analytically to reveal that at steady state, mean tail length is a function of the ratio between degradation rate and deadenylation rate, but independent of production rates (**Fig. 2B**, Material & Methods). Importantly, this relationship is robust to relaxation of the two key assumptions of the model **(Fig. S4 and Supplemental Note 1)**. An important insight from this theoretical model is that for any given mRNA, the distribution (and hence also the average) of long-tailed transcripts (i.e. transcripts with tail length $>A_{min}$) is uniform, determined by A_{max} and A_{min}, but independent of deadenylation and degradation rates. Instead, changes in deadenylation and degradation can modulate the *fraction* of short tailed transcripts, and only in this manner impact mean tail length. Increased deadenylation rates give rise to a smaller fraction of long-tailed transcripts, hence decreasing the mean tail length **(Fig. 2C-D center)**. Conversely, increased degradation rates decrease the fraction of short-tailed transcripts, hence increasing the mean tail length **(Fig. 2C-D right)**. Changes in the production rate do not impact either of the two fractions and hence do not impact mean tail length **(Fig. 2C-D left)**. As a consequence of this interplay between deadenylation and degradation rates, genes with orders of magnitude differences in either of the rates can have similar mean tail length, as long as the degradation to deadenylation ratio remains similar (**Fig. S5A**).

A testable prediction of this model is that the fraction of short-tailed transcripts should be inversely proportional to the mean tail length. To test this, we calculated for each gene the 'fraction of short-tailed transcripts', defined as the fraction of transcripts with a tail < 20 nt. Supporting our model's assumptions, we observed an excellent agreement between the mean tail length and the fraction of short-tailed transcripts ($\rho \sim 0.8$, **Fig. S5B**). These observations could be further reinforced by directly examining the distributions of tail lengths in mitosis and meiosis, which gave rise to two observations: First, consistent with the model, we observed evidence for a bimodal distribution, with one prominent peak at a length of around 20 bp and a broader peak at around 50bp **(Fig. 2E, Top)**.However, while our model predicts a completely flatted distribution of the long tailed fraction of molecules we detect a mild reduction of molecules in correlation with tail length, which can be explained via relaxation of some of the assumptions of the model **(Fig. S4 and Supplemental Note 1)**. Second, revisiting the association between tail length and mean transcript length, we found that transcript length displayed a strong correlation with the fraction of short tailed transcripts specifically in meiosis ($\rho=0.5$) but not under vegetative conditions ($\rho=0.06$) **(Fig. 2E Bottom, 2F)**. These findings thus demonstrate that the reshaping of poly(A) tail profile is triggered by meiosis-specific changes in the fraction of short-tailed transcripts, in a manner strongly associated with transcript length.

Combination of modeling with perturbational assays suggests decoupling of degradation from deadenylation in yeast meiosis

With this analytic framework at hand, we next explored the possible scenarios that could give rise to the experimentally observed transcript-tail correlation. Given that changes in mean poly(A) tail length can only be affected by changes in β (deadenylation) and/or γ (degradation), we identified 17 modules outlining all possible architectural configurations in which transcript length impacts β and/or γ either positively or negatively **(Fig. S5C)**. These modules could be grouped into three general configurations: 1) Transcript length impacts at most one of the rates (modules #1-5), 2) Transcript length affects both rates independently (modules #6-9), and 3) Transcript length impacts both rates dependently on on another (modules #10-17) **(Fig. S5C)**. We then associated each of these 17 modules with the predicted qualitative (positive / negative / absence) association between transcript length and mean poly(A) tail length, based on our analytic framework. For example, under module #8, transcript length positively regulates deadenylation rate and negatively regulates degradation rate. Given that each of these two modes of regulation independently result in decreasing mean poly(A) tail length, under this module, transcript length will negatively correlate with mean poly(A) tail length. Based on this analysis, out of the 17 modules we analysed, only 7 are consistent with having no correlation between transcript and tail lengths, as observed under vegetative growth conditions **(Fig. 3A)**. In order to determine which of these modules models the biological system, we noted that each module provides distinct predictions in response to deletion of the deadenylase machinery and the degradation machinery **(Fig. 3A)**. For instance, modules #6 and #7 both give rise to no correlation under unperturbed conditions, but following deletion of the deadenylation machinery module #6 will yield a positive correlation between the two whereas module #7 will yield a negative correlation. Interestingly, negative correlations between transcript length and poly(A) tail length (as appear in meiosis) are predicted under diverse perturbations. Experimental perturbations of the degradation and deadenylation machineries should allow both to dissect the regulatory configuration under mitotic conditions, and shed light on the changes occurring in meiosis.

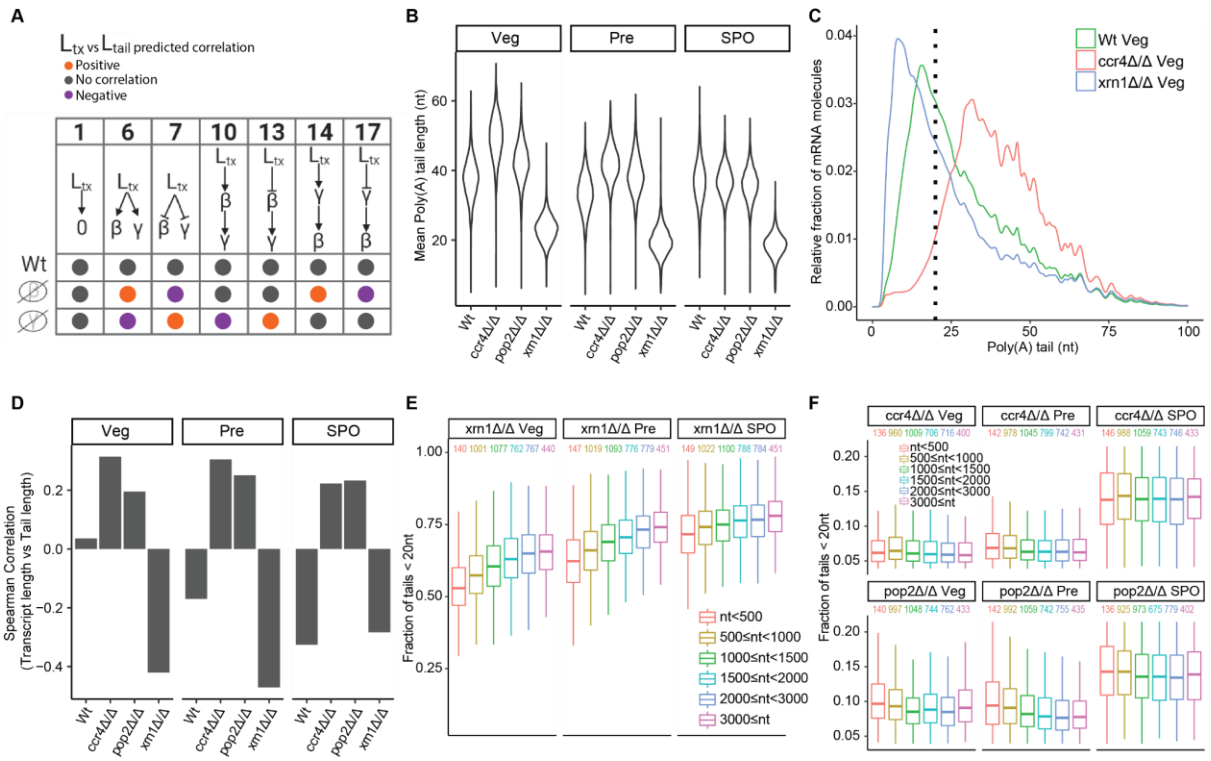

Figure 3. Combination of modeling with perturbational assays shows decoupling of degradation from deadenylation in yeast meiosis. A) The subset of regulatory modules (of 17 possible modules) that are predicted by the model to give rise to an absence of a correlation between transcript length (L_{tx}) and mean poly(A) tail length (L_{tail}), as observed under vegetative conditions. The panel further qualitatively depicts the nature of correlation

(positive(orange), negative(purple), absence(grey)) that would arise, for each architecture, following loss of deadenylation (β) or degradation (γ) activity. **B)** Violin plot of genes mean poly(A) tail length in the Wt, ccr4Δ/Δ, pop2Δ/Δ and xrn1Δ/Δ strains in vegetative growth, premeiotic and after 5 hrs in SPO conditions. **C)** Tail length distributions of mRNA molecules of the Wt, ccr4Δ/Δ and the xrn1Δ/Δ strain in vegetative growth. A dashed line was drawn at 20nt. **D)** Barplot showing Spearman correlation between genes mean poly(A) tail length and log2 of transcript length. **E)** Boxplot of the fraction of tails under 20nt per genes divided by transcript length groups at each timepoint for the xrn1Δ/Δ strain. Number of genes per group is indicated with the corresponding specific color. **F)** Similar to E but for ccr4Δ/Δ and pop2Δ/Δ strains.

To distinguish between the different models, we began by perturbing the degradation rate (γ), by knocking out Xrn1, which mediates 5'-to-3' degradation of deadenylated mRNAs [37]. We generated an xrn1Δ/Δ strain, induced meiosis and measured poly(A) tails during vegetative growth, premeiotic stage, and after 5 hrs in SPO. Yeast lacking Xrn1 had a reduced sporulation capacity (~11% of cells form spores, in comparison to ~90% in WT cells) **(Fig. S2C)**, and exhibited a delay already in premeiotic DNA replication **(Fig. S2A)**. Consistent with the predictions by our model, deletion of Xrn1 (reduced degradation, γ) caused a massive accumulation of short tailed transcripts **(Fig. 3B,C)**, resulting in a ~40% decrease in the average of the mean tail length. Remarkably, loss of Xrn1 also resulted in a negative correlation between poly(A) tail length and transcript length under both vegetative growth and premeiotic conditions **(Fig. 3D),** both of which lack this correlation under unperturbed conditions. Moreover, the fraction of short-tailed transcripts per gene correlated well between meiosis conditions and xrn1Δ/Δ cells in vegetative growth phase **(Fig. S6A right).** Meiotic poly(A) tail profiles can thus be phenocopied by depleting vegetative growth cells of Xrn1. To further confirm this result and avoid potential compensatory mechanisms activated in the xrn1Δ/Δ yeast, we fused Xrn1 to an auxin-inducible degron, allowing to rapidly decrease Xrn1 protein levels in the presence of auxin [38]. Within 30 minutes of activating the degron, we already detected a reduction of tail length, negative correlation with transcript length and an accumulation of short tails associated with transcript length **(Fig. S6B)**.

These observations have four important implications. First, they are congruent with our model, based on which decreased degradation rate results in a higher proportion of short-tailed transcripts, thereby reducing mean tail lengths. Second, these results suggest that preferential deadenylation in longer genes occurs not only in meiosis but also under vegetative growth conditions - but that under such conditions short tailed transcripts are subjected to rapid Xrn1-mediated elimination. Third, the fact that Xrn1-depleted nutrient rich conditions phenocopies meiotic conditions suggests that Xrn1 activity and/or its coupling to deadenylation may be altered in meiosis. Finally, the measurements of tail-transcript length associations following perturbation of Xrn1 allowed us to narrow down the set of relevant network configurations to modules #6 and #10 **(Fig. 3A)**, both of which give rise to negative correlation when degradation rate is perturbed.

To distinguish between modules #6 and #10, we next perturbed the deadenylation rate (β), by deleting the two primary deadenylases, Ccr4 and Pop2. We induced meiosis in each of these strains, monitored via nuclear staining and FACS, and measured poly(A) tail length under vegetative growth, premeiotic stage and after 5 hours following induction of sporulation. Interestingly, while these two deadenylases are not essential for mitosis, we found that they are required for meiosis, as even premeiotic DNA replication did not occur as late as 9 hours after induction of sporulation **(Fig. S2A)**, and no spores were observed 24 hours after sporulation induction **(Fig. S2C)**. Different members of the CCR4-NOT complex have also been reported to be essential for proper meiosis in *D. melanogaster* [39], *C.elegans* [40] and mice [41], highlighting the importance of poly(A) tail regulation for proper meiotic progression.

Consistent with our analytical model, deadenylation mutants exhibited a decreased fraction of short-tailed transcripts **(Fig. 3C, Fig. S6C-D),** resulting in a roughly 10-nt increase in the average of mean poly(A) tails in comparison with the WT. These differences were consistently observed under vegetative growth and premeiotic conditions, but - for reasons remaining unclear to us (see Discussion) - not under meiotic conditions **(Fig. 3B,C)**. Deletion of each of the two deadenylases resulted in an abolishment of

the negative tail-transcript association under both pre-meiotic and meiotic conditions and its replacement by a weak positive correlation (ρ~0.2) **(Fig. 3D)**. This weak correlation renders it difficult to distinguish module #6 (in which a positive correlation is expected) from module #10 (in which no correlation would be expected). To further attempt to distinguish between modules #6 and #10, we sought to *increase* deadenylation activity, by overexpressing Ccr4 under vegetative growth conditions [42]. Under this scenario, module #6 predicts the emergence of a negative correlation between transcript length and poly(A) tail due to the preferential reduction of long tailed transcripts fraction in longer genes. In contrast, under module #10, in which any change in deadenylation will drive a proportional change in degradation, no transcript length-poly(A) tail correlation should be detected. Despite the accumulation of short tails due to a roughly 32-fold induction of Ccr4 transcript levels **(Fig. S7A)**, no correlation between transcript length and poly(A) tail length is observed **(Fig. S7B-C),** thereby providing support for module #10. Based on this experiment and theoretical considerations our results are suggestive of module #10, but could also potentially point at a 'hybrid' module sharing characteristics of both (see 'Discussion'). This notwithstanding, it should be highlighted that modules #6 and #10 are quite similar. In both cases transcript length directly and positively regulates deadenylation rate and is positively associated with degradation rate. Yet, in module #6 transcript length directly mediates degradation rate and in module #10 the impact on degradation rate is indirect, and mediated via control of the deadenylation rate **(Fig. 3A)**.

Importantly, we found that upon loss of the two deadenylases, the propensity for short-tailed transcripts to form is no longer associated with transcript length **(Fig. 3F)**, in stark contrast to WT meiosis conditions or loss of Xrn1 under nutrient rich conditions **(Figs. 2E-F, 3E)**. These results suggest that the preferential accumulation of short tails observed under meiosis conditions or in the absence of Xrn1 is a consequence of preferential targeting of longer transcripts by deadenylases (which can hence be abrogated by deletion of the deadenylases **(Fig. 3B)**. Thus, the opposing effects of deadenylation rate and degradation rate mask the correlation between transcript length and deadenylation in vegetative growth conditions, whereas decoupling of these rates under meiosis conditions or upon loss of Xrn1 leads to the emergence of a transcript length-poly(A) tail association.

Decoupling of degradation from deadenylation during meiosis triggers an association between gene expression and tail length

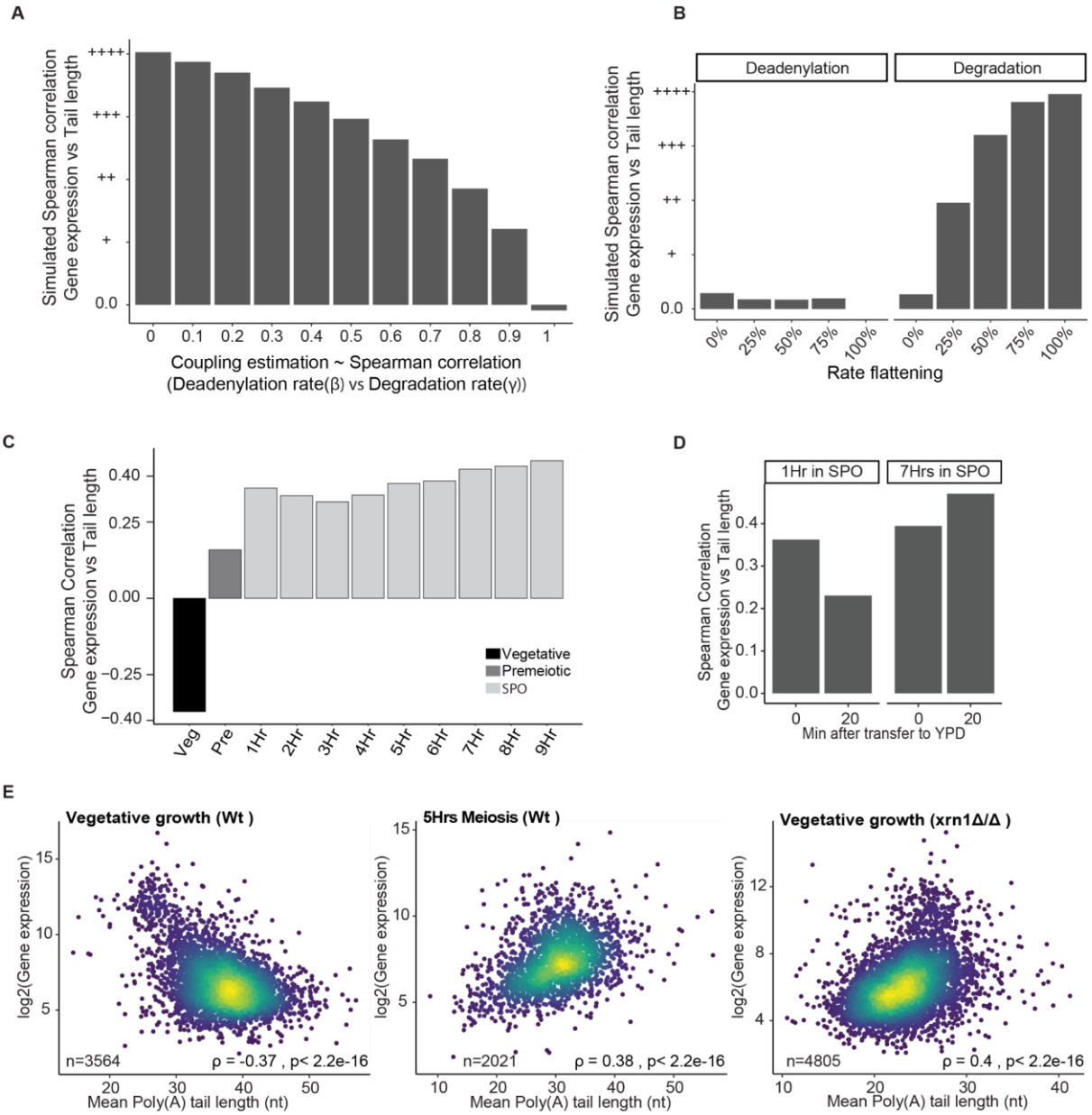

Figure 4. Decoupling of degradation from deadenylation during meiosis triggers an association between gene expression and tail length. A) Barplot showing the simulated correlation between mean poly(A) tail length and gene expression at constant production with different degrees of coupling between deadenylation rate and degradation rate, estimated as the correlation between both rates. Barplot showing the simulated correlation between mean poly(A) tail length and gene expression at constant production when deadenylation and degradation rates are flattened to different extents.**C)** Barplot showing the Spearman correlation between the log2 of normalized gene expression vs mean tail length across the meiotic time course. **D)** Barplot showing Spearman correlation between genes mean poly(A) tail length and log2 of transcript length uncommitted (1hr in SPO) and committed (7 hrs in SPO) to meiosis cells before and after transfer to YPD. **E)** Scatterplots of the poly(A) tail length vs log2 of normalized gene expression in the Wt in vegetative growth (Left) meiosis (Center) and xrn1Δ/Δ in vegetative growth (Right).The figure was generated like in Fig. 1D.

It was recently demonstrated that under many profiled conditions, there is no association between gene expression levels and poly(A) tail length, due to the coupling of deadenylation rates to degradation rates [9]. To predict how decoupling or perturbations in either of the rates affects this relationship we simulated the effect of decoupling by generating pairs of deadenylation and degradation values at different degrees of correlation, and based on our model calculated mean poly(A) tail length and gene expression. The extent of correlation between mean poly(A) tail and gene expression decreased as

degradation and deadenylation were more coupled **(Fig. 4A).** Thus, under vegetative conditions no correlation between the two is expected, whereas under decoupled scenarios, such as in meiosis, a positive correlation is anticipated. In addition, we simulated the impact of Xrn1 and Ccr4/Pop2 deletion in this interaction, by flattening either of the rates to different extents, with the assumption - guided by module #10 - that degradation is triggered by deadenylation. Flattening of degradation gave rise to a positive correlation between tail length and gene expression **(Fig. 4B)**, whereas flattening of deadenylation rates did not result in a correlation. Thus, these simulations anticipate a positive relationship, even under vegetative conditions, upon depletion of Xrn1. Consistent with these predictions, inspection of gene expression as a function of poly(A) tail length revealed a striking positive correlation exclusively in meiosis **(Fig. 4C)**. On the other hand, in mitosis we detected a negative correlation, which is inconsistent with our model. However, this correlation is driven by a subset of highly expressed genes and is eliminated once these are excluded **(Fig. S8).** This may suggest a more complex regulatory scheme to which a small number of highly-expressed genes is subjected, potentially consistent with previous reports [43]. Also in congruence with our model, the positive correlation was (1) rapidly decreased upon return to growth experiment in uncommitted cells **(Fig. 4D)**, (2) maintained in a return to growth experiment in committed cells **(Fig. 4D)**, and (3) could be reproduced under vegetative conditions in xrn1Δ/Δ strain **(Fig. 4E)**. Thus, in all of the contexts in which a negative tail-transcript correlation was established, a positive correlation was established between tail-length and gene expression. These results thus demonstrate how the decoupling between deadenylation and degradation can lead to reshaping of poly(A) tails of expressed genes, leading to a unique association between gene expression profiles and tail lengths.

Xrn1 foci formation are associated with the emergence of a poly(A) tail - transcript length interaction

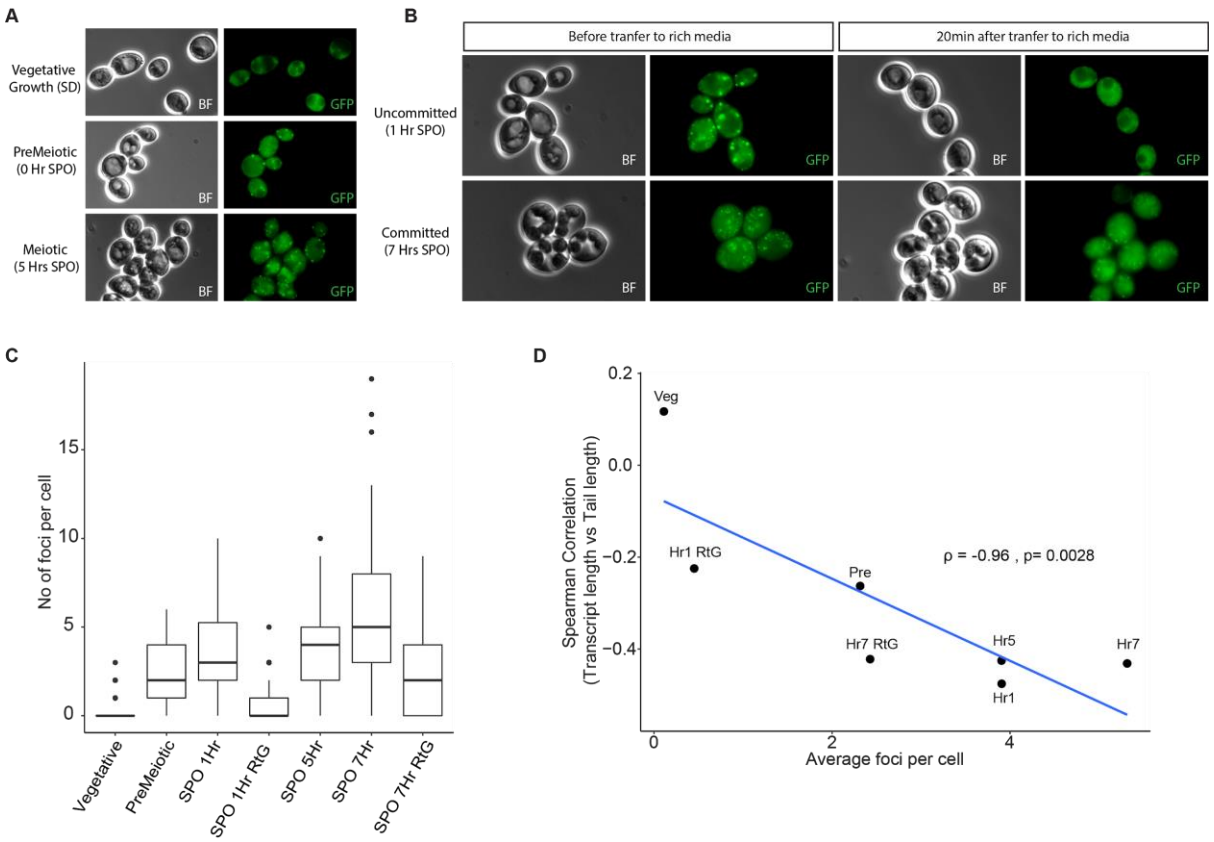

Figure 5. Xrn1 foci formation is connected to poly(A) tail - transcript length interaction. A) Representative images of the Xrn1 subcellular localization across meiosis induction. GFP (Green) and brightfield (BF) are displayed **B)** Representative images of the Xrn1 subcellular localization across return to growth experiments in uncommitted and committed cells. **C)** Boxplot showing Xrn1 foci quantification, a minimum of 100 cells was

quantified per point. **D)** Scatter plot of transcript length- poly(A) tail length spearman correlation vs average foci per cells across conditions. Spearman correlation was calculated.

Our results thus far suggested that during meiosis, degradation is decoupled from deadenylation. Such decoupling could either be caused by reduced activity of Xrn1 or by preventing a potential interaction between the deadenylation and degradation machineries. Because no major differences in the average of the mean tail length between vegetative growth and meiotic conditions are observed, a general reduction in Xrn1 activity is unlikely (**Fig. 3B)**. To evaluate this, we assessed RNA and protein levels of Xrn1, in addition to several other proteins involved in the 5'-to-3' degradation (Dcp1,Dcp2, Edc1,Edc3 and Dhh1), based on detailed measurements obtained by Cheng et al. over multiple timepoints in meiosis [26]. Only minor differences in expression between vegetative and meiotic conditions were observed for the selected genes **(Fig. S9)** supporting the hypothesis that the decoupling is not caused by a major reduction in degradation rates.

Motivated by previous works demonstrating that Xrn1 can relocalize into processing bodies (P-bodies) upon different stimuli including meiosis [44–46], we next examined the subcellular localization of a GFP-tagged Xrn1 allele in meiosis. Under vegetative growth conditions, Xrn1 displayed a diffuse staining pattern predominantly within the cytoplasm. Upon induction of meiosis, Xrn1 relocalized into highly distinct foci **(Fig. 5A, Fig. 5C)**. We further assessed Xrn1 localization in the context of a return-to-growth experiment, in both committed and uncommitted cells, to assess whether focal staining patterns of Xrn1 would be exclusive to committed, but not to uncommitted cells, mirroring the transcript-tail association **(Fig. S3D)**. Indeed, we found that uncommitted cells (1hr in SPO) transferred into rich media completely lost Xrn1 foci **(Fig. 5B,Fig. 5C),** whereas these foci are maintained in committed cells (7 hr in SPO). A joint analysis of the meiosis and return to growth experiment thus reveals an excellent correlation between the number of Xrn1 foci per cell and the magnitude of the transcript-tail correlation **(Fig. 5D)**, suggesting that this focal localization pattern may play a causative role in the decoupling of degradation from deadenylation.

Transcript length impact on deadenylation is conserved in mammals

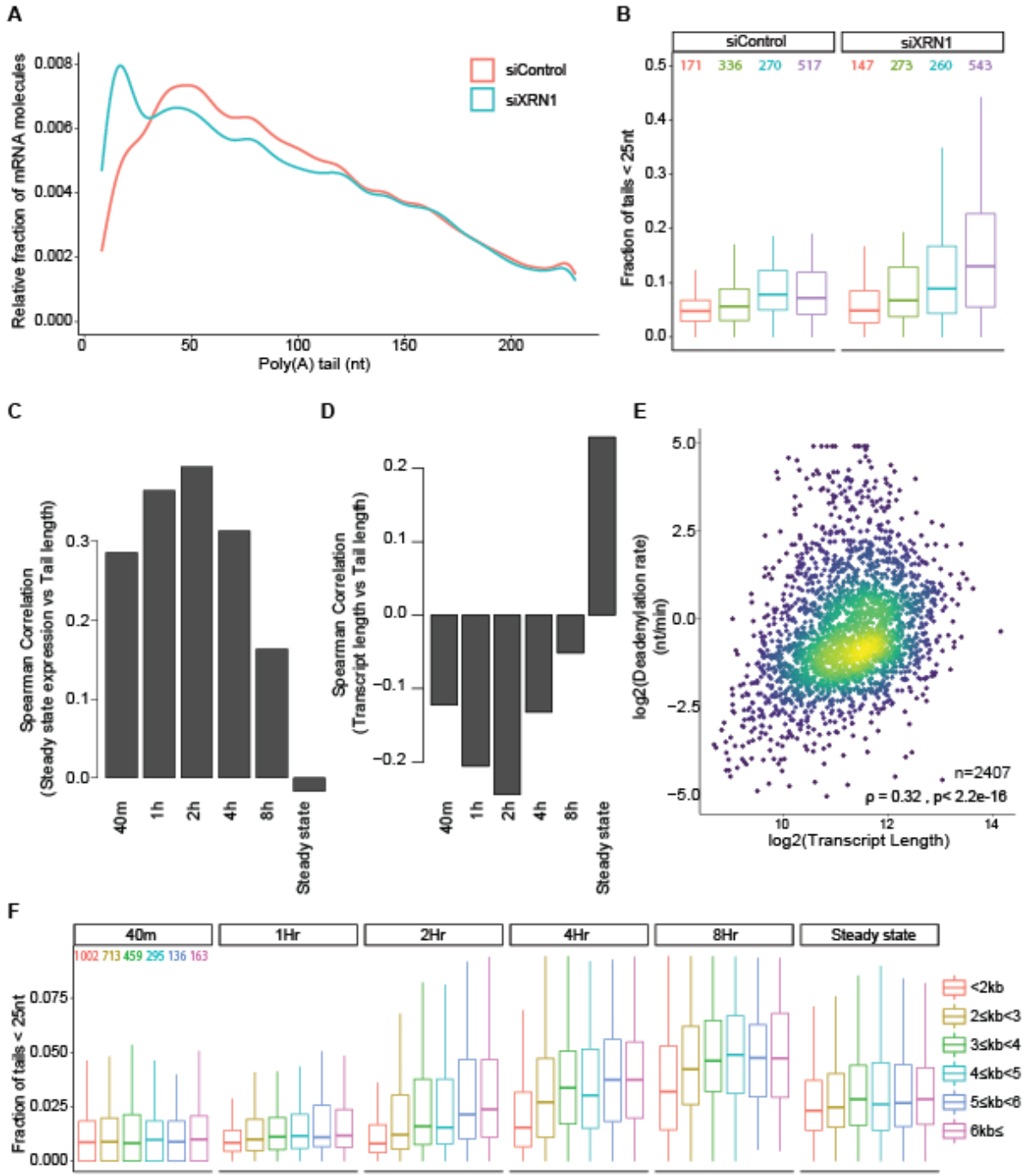

Figure 6. Transcript length impact in deadenylation is conserved in mammals. A) Tail length distributions of mRNA molecules in Hela cells transfected with control siRNA (siControl) (left) or XRN1 siRNA (siXRN1) (right) from [47]. **B)** Boxplot of the fraction of tails under 25nt per genes and plotted by transcript length groups across timepoints for tails in siControl and siXRN1. Number of genes per group is indicated with the corresponding specific color. **C)** Barplot of Spearman correlation between poly(A) tail length data from [9] metabolic labeling time course in 3T3 cells and the log2 of steady state expression. **D)** Similar to C but vs the log2 of transcript length. **E)** Scatterplot of the log2 of the deadenylation rate and the log2 of transcript length. The figure was generated like in Fig. 1D. **F)** Boxplot of the fraction of tails under 25nt per genes and plotted by transcript length groups across timepoints. Number of genes per group is indicated with the corresponding specific color in the first timepoint.

To evaluate if transcript length is an evolutionarily conserved determinant of deadenylation, we first reanalysed poly(A) tail measurements obtained in Hela cells in which XRN1 had been knocked down via siRNA [23]. In concordance with the published results [23] and our results in yeast, siXRN1 showed

accumulation of short tails compared with siControl **(Fig. 6A)**. Moreover, as in yeast, Xrn1 knockdown led to a preferential accumulation of short tailed transcripts (tails <25 nt) in longer genes **(Fig. 6B).** These results hence suggest that in mammals, as in yeast, deadenylation rates are governed by transcript length.

To further explore this, we next reanalyzed poly(A) tail measurements that had been acquired in 3T3 mouse cells at multiple timepoints following metabolic labelling [9], i.e. within populations of transcripts that have not yet reached steady state. Thus, within these populations of nascent RNAs, deadenylation and degradation are decoupled, given that in these populations tails are subjected to partial deadenylation but not yet to degradation. Consistently with the reported findings [9], we could recapitulate that at 2 hours following labelling - but not at steady state - tail lengths were well correlated with gene expression levels (**Fig. 6C**). Analyzing this dataset from the perspective of transcript length, we observed a negative association between transcript length and poly(A) tail length peaking at precisely the same 2 hr timepoint, and eliminated at steady state **(Fig. 6D)**. Consistently, transcript length correlated positively with the deadenylation rates that had been inferred in this study **(Fig. 6E).** In contrast, transcript length did not correlate with initial poly(A) tail lengths, and displayed a low positive correlation with deadenylated-transcript degradation rates **(Fig. S10A-B)**. As in yeast meiosis, this correlation was driven by the accumulation of short-tailed (tails <25 nt) transcripts of longer genes, which was apparent at 2 and 4 hour timepoints, but not at steady state **(Fig. 6F)**. Thus, as in yeast meiosis, at the precise timepoints at which a negative correlation can be observed between poly(A) tail length and transcript length, a positive correlation is observed between the length of poly(A) tails and expression levels. This set of results, based both on genetic decoupling of degradation from deadenylation and on populations of nascent RNAs, thus provides additional evidence for the association of transcript length with deadenylation rates in mammalian species.

Discussion

In this study we developed an approach allowing systematic, robust and multiplexed quantification of poly(A) tails, which we applied to up to 12 samples in parallel. This approach allowed us to discover a unique physiological context, yeast meiosis, in which mRNA deadenylation and degradation rates are decoupled. Our findings add an important dimension to a previous study conducted in cell lines inferring that degradation and deadenylation rates are coupled [9], and demonstrates that there are regimes in which the two undergo uncoupling. We demonstrate that such regimes can also be phenocopied genetically or via metabolic labelling, and under all of these a strong association is observed between transcript length and the fraction of short tailed transcripts, giving rise to an inverse correlation with poly(A) tail length. These associations are all lost in a coupled regime **(Fig. 7)**. To our knowledge, this report is the first to document a global decoupling between deadenylation and degradation. Interestingly, a deadenylated reporter RNA in Xenopus oocytes was also found not to undergo degradation [48], suggesting that also within this system deadenylation and degradation can be decoupled, at least to some extent. The fact that such decoupling is observed both in yeast and in oocytes undergoing meiosis is intriguing, and could point at a conserved role for such decoupling.

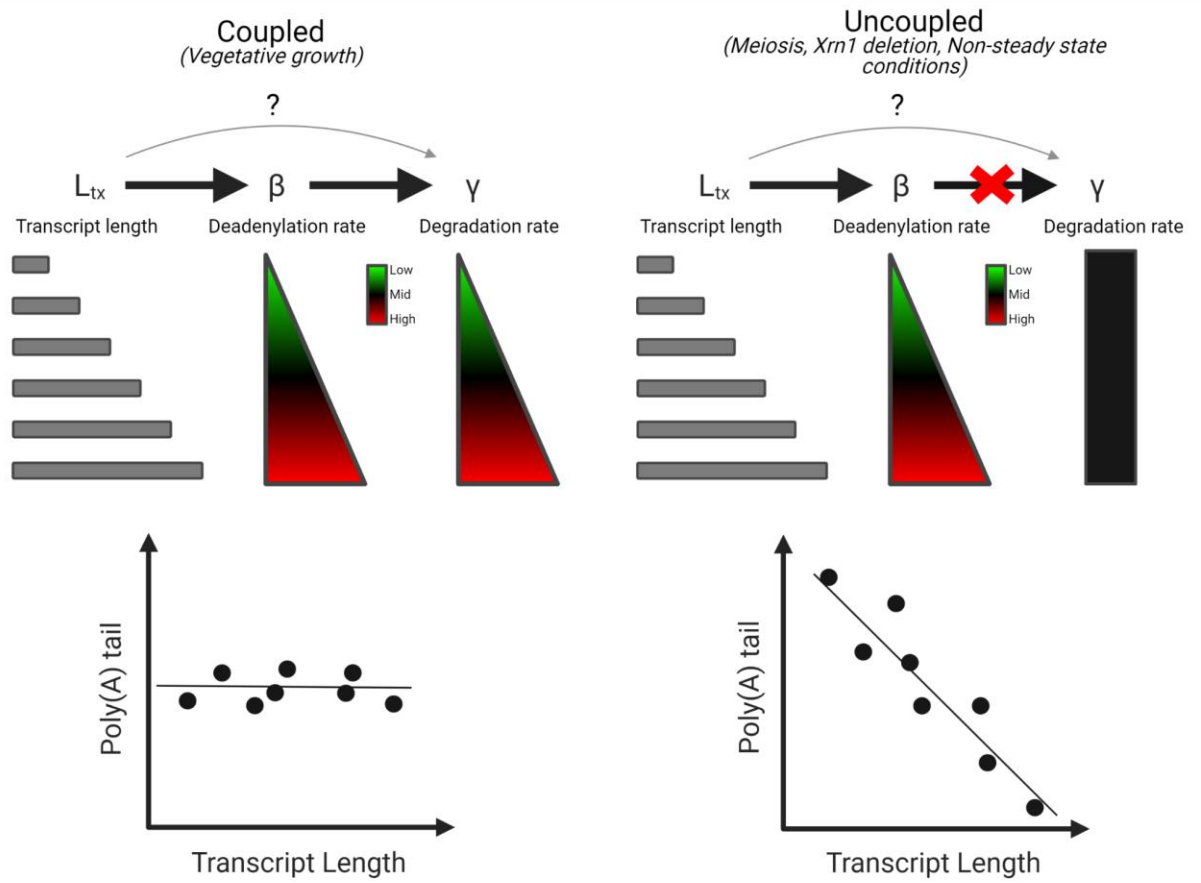

Figure 7. Poly(A) tail regulation in coupled and uncoupled regimes. In coupled regimes, like yeast vegetative growth, transcript length positively impacts degradation rate (γ) mostly through deadenylation rate (β) but potentially also to a low extent also independently of deadenylation rate (see 'Discussion'). Consequently no correlation between transcript length and poly(A) tail is observed. In uncoupled regimes, like yeast meiosis, Xrn1 deprived cells or RNA under non-steady state conditions, the impact of transcript length on deadenylation rate is maintained but the link with degradation rate is disrupted, leading to a negative correlation between the transcript length and poly(A) tail length.

Due to the opposing effects on tail-length exerted by deadenylation and degradation, and the correlation between these two rates, interpretation of changes in tail-length is complex. Our results highlight the importance of analyzing the entire *distribution* of tail-length per transcript (rather than only the mean tail length) and of interpreting these measurements in the context of a mathematical model which we developed based on [9]. An interesting insight from this model is that the key parameter that needs to be estimated - in order to infer relative changes in deadenylation versus degradation - is the fraction of short-tailed transcripts. Thus, under conditions in which this model holds, it is not necessary to precisely quantify the poly(A) tails length - which, in particular in mammalian contexts, remain subject to technical limitations, and instead it is merely necessary to quantify the fraction of tails shorter than ~25 bp. Thus, these insights suggest that our experimental approach is relevant for inference of changes in deadenylation versus degradation kinetics not only in organisms with relatively short poly(A) tails, as in yeast, but also in mammalian contexts.

A key result in our study is the inferred association between transcript length and deadenylation rates. Based on our modeling and perturbational studies, we converged on one of two similar yet distinct architectures. Based on the first architecture (module #10, **Fig. 3A**), transcript lengths positively regulate deadenylation rates, which *in turn* positively impact degradation rate. Based on the second architecture (module #6, **Fig. 3A**), transcript length *directly* positively regulates both deadenylation and degradation rate. Distinguishing between these modules is rendered difficult, given that the

experimental results partially support both. In support of module #6, loss of Ccr4 results in a slightly positive association between transcript and tail length, whereas module #10 would predict a complete loss of the association. However, in support of module #10, overexpression of Ccr4 under vegetative conditions does not give rise to a negative correlation, as would be predicted by module #6. Moreover, in mice - where deadenylation and degradation rates were directly inferred - transcript length correlates substantially with deadenylation rates (ρ=0.32) but much more poorly with degradation rates (ρ=0.12). Potentially reconciling these observations, it is possible that in practice tail lengths are governed by a 'hybrid' architecture, on the basis of architecture #10, but with the addition of a weak, direct link between transcript length and degradation (as in module #6) **(Fig. 7)**. This architecture would be consistent with all of the above observations. Such a module is also consistent with observations that the difference in mean poly(A) tail length between WT and Ccr4/Pop2 mutants correlates positively with transcript length under both vegetative and meiosis contexts **(Fig. S11)**, which would not be expected purely based on module #10**.** We should further highlight that from a theoretical standpoint, a module in which deadenylation rates *govern* degradation rates (such as in module #10 or, to a large extent, in the hybrid module) is expected to be more robust, because any sources of variability impacting deadenylation would automatically also affect degradation, resulting in maintenance of the original mean poly(A) tail length. In contrast, to maintain a constant poly(A) tail length based purely on module #6, any transcript-length-dependent factor impacting deadenylation rate must - independently, through a different mechanism - impact degradation rate to an identical degree.

We also considered an alternative model in which the basis for accumulation of short-tails within longer genes is attributed to the longer duration of degradation for longer genes. Based on this model, the preferential accumulation of short tails within longer genes could simply reflect an abundance of deadenylated but not fully degraded segments originating from longer genes, rather than higher deadenylation rates. mPAT-seq does not distinguish full length mRNA molecules from degradation intermediates, rendering it challenging to distinguish one model from the other based on the poly(A) tail data. However, this model predicts the presence of 5'-->3' degradation intermediates and 3' fragments of endonucleolytic cleavage, in particular within longer genes, causing a significant 3' bias in coverage among genes. To assess whether this was the case, we applied RNA-seq following ribosome depletion. We observed no global 3' bias in the data, nor any *per gene* correlation between gene length and extent of 3' bias **(Fig. S12)**. We therefore consider such a model unlikely.

An important limitation in our study is that due to technical difficulties, we are unable to directly measure deadenylation and degradation rates, and instead can only infer *differences in their relative levels* based on steady state lengths of poly(A). A consequence of this is that the precise nature of the "decoupling" of these two rates remains to be explored. One possibility is that degradation rates are distributed across genes independently of deadenylation rates. A second alternative is that degradation rates converge to a relatively fixed range across all genes (i.e. degradation rates become 'constant' across all genes). From a functional perspective, a fixed degradation rate (the latter scenario) may allow rapid reshaping of the transcriptome without requiring changes in transcription, given that it would give rise to upregulation of highly deadenylated genes and downregulation of lowly deadenylated genes, hence flattening the variability of gene expression (between genes). Consistently with this scenario, we observe ~15% decrease in the standard deviation of gene expression levels in meiosis and in the Xrn1 deletion. Moreover, variability is recovered in uncommitted cells after transfer to rich media but not in committed cells **(Fig. S13)**. Interestingly, a gene ontology (GO) analysis reveals that genes with shrinking tails are enriched for genes involved in mitotic growth while genes with expanding tails are enriched in oxidative respiration, which is critical for proper meiosis (but not mitosis) [49–51] **(Fig. S14)**. In this manner, changes in gene expression induced by decoupling of degradation from deadenylation could potentially reshape gene expression to facilitate an expression program required for meiosis.

Our model does not fully account for all of our observations. In particular, our model cannot explain the accumulation of short tails in ccr4Δ/Δ and pop2Δ/Δ strains after induction of meiosis **(Fig. 3F).** It is

possible that specifically in uncoupled regimes, such as in meiosis, compensatory mechanisms are triggered by deletion of the deadenylases reducing degradation activity. In addition, several reports challenge some of the model's general assumptions. First, cases of cytoplasmic deadenylation [52] have been reported in higher eukaryotes altering the unique production event at A_{max} length. Second, factors that disrupt a monotonic deadenylation, including poly(A) tail modifications [47,53], PAB1 signature patterns [23] and biphasic deadenylation performed by different deadenylases [54] would alter the distribution of long tails predicted by our model. Also, events of coupling between transcription and degradation [55,56] are inconsistent with our model in which deadenylation and degradation rates are independent of production.

What is the mechanism underlying the association between transcript length and deadenylation? The fact that this association can be eliminated by deletion of either Ccr4 or Pop2 strongly implicates these factors in the mediation of this process. Yet, the mechanistic basis for this association remains to be discovered. To dissect this question it will be crucial to understand how and whether transcript length can be 'sensed'. One intriguing possibility is that transcript length could directly impact the deadenylation kinetics, for example by impacting circularization efficiency which is negatively influenced by transcript length [57]. Alternatively, transcript length can be 'sensed' indirectly. For example, deadenylation activity could reflect the joint destabilizing activity of multiple RNA binding proteins that associate with a transcript, resulting in increased susceptibility to deadenylation of longer transcripts, given that they offer more binding sites to diverse RNA binding proteins.

An additional open question pertains to the mechanistic basis for the coupling between deadenylation and degradation [9,58]. Our results associate the decoupling of the two to the formation of Xrn1 foci, which could suggest that under 'coupled' regimes Xrn1 is physically located elsewhere in the cytoplasm where it can potentially interact with deadenylation factors, giving rise to the observed coupling. Indeed, in mammalian systems, Xrn1 physically interacts with members of the CCR4-NOT complex [59] which might be critical for the coupling of both steps. Such coupling may also be mediated through interacting partners, as suggested by the presence of several proteins that are physically associated with members of the CCR4-NOT complex and decay related proteins [60–62].

The development of a scalable sequencing approach for measurement of the poly(A) tail length, genetic perturbations and modeling allowed us to uncover a unique case in which deadenylation and degradation underwent decoupling, allowing us to discover a relation between the two and transcript length. It will be of interest in the future to employ these approaches to understand to what extent these observations form a rule or an exception.

Materials and methods:

Strains and growth conditions:

All yeast strains used in this work were derived from the sporulation proficient SK1 strain background (**Table 1**). ccr4Δ/Δ, pop2Δ/Δ and xrn1Δ/Δ deletion strains were obtained by deleting the genes with hphMX, natMX or kanMX cassettes in haploid cells followed by mating and double selection. Similar transformation strategy was used to swap the Ccr4 promoter for the Cup1 inducible promoter and for 3' GFP tagging of Xrn1. All vegetative growth points were growing cells at 30°C at 190 rpm in YPD 2% (1% yeast extract, 2% peptone, 2% dextrose), or SD (2% dextrose, 0.67% Difco yeast nitrogen base without amino acids, and amino acids as required) for imaging,and taken after reaching OD600 = ~0.5. To induce synchronous meiotic entry, cells were grown for 24 h in YPD 4% (1% yeast extract, 2% peptone, 4% dextrose) at 30°C, diluted in BYTA (1% yeast extract, 2% tryptone, 1% potassium acetate, 50 mM potassium phthalate) to OD600 = 0.2 and grown for another 16 h at 30°C, 200 rpm. Cells were then washed twice with water, re-suspended in SPO (0.3% potassium acetate) at OD600 = 2.0 and incubated at 30°C at 190 rpm. For the return to growth experiment cells were removed from SPO at

indicated timepoints and resuspended in YPD 2% for RNA extraction, SD for imaging or into Glucose 4% for spores quantification after 24 h incubation. Xrn1 degron system was activated by adding 500µM auxin/Indole-3-acetic acid(IAA) + 50µM CuSo4 to the inducible strain at OD600 = ~0.5. Overexpression of Ccr4 was caused by activating the Cup1 promoter with 50µM CuSo4 to the inducible strain at OD600 = 0.5. Cells were isolated from each media at the indicated times and collected by 2 min centrifugation at 3000 g. Pellets were snap-frozen and stored at -80°C for RNA extraction. To observe the progression in cell meiosis, a sample of cells was taken at each timepoint during sporulation for DAPI staining and Flow Cytometry - DNA staining quantification (below).

Dapi staining and spores quantification:

Cells were first fixed by Formaldehyde overnight (J.T Baker, UN2209). followed by a first 5 min incubation with KPO_4/sorbitol plus 1%Triton-X and second 5min incubation with KPO_4/sorbitol plus DAPI, dilactate (ThermoScientific, D3571). Spores were quantified after 24 h in SPO or Glucose 4%. A minimum of 100 cells were quantified at each timepoint. Cells were observed by Zeiss Axiolmager M2 Fluorescent microscope system.

Flow Cytometry – DNA staining

Cells were washed twice with 50mM Tris-HCl pH 8.0, re-suspended in RNase A for 40 minutes in 37°C, washed twice with 50mM Tris-HCl pH 8.0, and re-suspended in Proteinase K for 1-hour incubation at 37°C. Then, cells were washed twice again, re-suspended in SYBR green (1:1000) and incubated in the dark at room temperature for 1 hour. Next, the stain was washed from the cells, which were resuspended in 50mM Tris-HCl pH 8.0 and sonicated in Diagenode bioruptor for 3 cycles of 10'' ON and 20'' OFF in low intensity. Cells were analyzed using the FACS LSRII system (BD Biosciences).

Xrn1 sub-cellular localization and foci quantification

Cells were grown as indicated, to avoid self fluorescence YPD 2% was replaced with SD. At each timepoint a sample of cells were removed from the culture and immediately observed in the microscope. For foci number quantification a minimum of 100 cells was zevaluated at each timepoint.

RNA extraction:

Yeast 200nt<RNA samples were prepared by using a modified protocol of the NucleoSpin RNA mini kit (Macherey-Nagel, 740955.50) which size-selects transcripts longer than 200nt. Specifically, cell lysis was done by adding 450µL of lysis buffer containing 1M sorbitol (Sigma-Aldrich), 100mM EDTA, and 0.45µL lyticase (10 International units/µL). The samples were incubated for 30 min at 30°C to break the cell wall, then centrifuged for 10 min at 3000 rpm, and the supernatant was removed. From this stage, extraction proceeded as in the protocol of the NucleoSpin kit, only substituting β-mercaptoethanol with DTT.

RT-qPCR:

Quantitative reverse-transcription PCR (RT–qPCR) was performed to assess the relative induction of Ccr4. Reverse transcription of the extracted RNA at the indicated timepoints was performed with the High-Capacity cDNA Reverse Transcription Kit (Applied Biosystems, 436881), according to the manufacturer's protocol. cDNA was labelled with KAPA SYBR FAST (Roche, KK4605) and measured in the StepOne™ Real-Time PCR System (Applied Biosystems).Relative quantification was calculated using Act1 as an internal control. Primers are listed in **Table 3**.

mPAT-seq library preparation:

Starting material for the pooled poly(A) sequencing protocol was 400 ng per sample (with 12 samples), if more samples are used potentially less starting material would be needed. 3' RNA barcode adapter ligation was performed with 20 pmol of RNA ILL adapter (**Table 3**) and 36 U T4 RNA ligase 1 (NEB) for 1.5 h at room temperature for each sample. After every step, unless stated otherwise, a cleanup with Dynabeads® MyOne™ Silane was performed according to the protocol. Following the 3' ligation of barcoded RNA adapters, all samples were pooled for ribosomal depletion with Ribo-Zero Gold rRNA Removal Kit (Yeast) (Illumina, MRZY1324) according to the kit protocol. Final clean up was performed with RNA Clean & Concentrator kit (Zymo research, R1017) according to the kit protocol using the size selection option (>200nt). RNA fragmentation to ~200 nt fragment size was performed by adding RNase T1 (Thermo Fisher, EN0541) (0.2 International units/µL) in digest buffer (0.3M NaCl, Tris (pH7.5), for 10 min at room temperature. cDNA synthesis was performed using the rTd RT primer (**Table 3**) and SuperScript™ III Reverse Transcriptase. Alkaline RNA hydrolysis was carried out in 1 M NaOH in 70°C for 12 min. Illumina 5'adapter ligation was performed with 50 pmol 5iLL-22 adapter with 45U T4 RNA Ligase 1 for overnight incubation at room temperature. PCR enrichment was performed with KAPA HiFi PCR Kit (Roche) with the universal forward primer and the reverse primer containing the barcode. Spike-ins were amplified side by side with the samples. Amplified libraries were cleaned with AMPure XP beads (Agencourt, A63881), quantified using Qubit (Life Technologies) and the distribution of library size was determined by library electrophoresis in an E-gel EX agarose gel, 2% (Invitrogen).

mPAT-seq analysis:

Paired-end reads of mPAT-seq libraries were demultiplexed into individual samples, using an in-house python script which distributes reads into a sample FASTQ file according to the barcoded-sequence in read 2 (Pos 4-10). For RNA identification, read 1 was aligned with STAR **v2.5.3a** [63] to the SacCer3 reference genome with default parameters but limiting the intron length to 1000 nt ('–alignIntronMax 1000' parameter). Reads were assigned to genes using the 'closest' function from bedtools **v2.26.0** [64] and reads that were further than 500nt away from the open reading frame end were filtered. For poly(A) quantification, two filters were applied. 1) A minimum of 4 adenosines at the beginning of the read 2 was required. 2) Reads that aligned perfectly to the genome (STAR --alignEndsType EndToEnd '', "--alignIntronMax 1,--outFilterMismatchNmax 3) were removed from the analysis to avoid genomic encoded adenosines. Quantification of poly(A) tail length was performed with a sliding window strategy beginning from the end of read 2, using a 5 nt window and a 1 nt offset, with a requirement that at least 4 of the 5 nucleotides in the window are adenosines; The 5' end of the poly(A) tail was defined as the 3'-most adenosine within the first window in which this condition was not fulfilled. A minimum of 30 poly(A) tags per gene were required for further analyses.

A similar strategy was used for spike-ins (**Table 2**). Using an in-house python **v2.7.12** script we obtained spike-in identity from read 1, by precisely matching the presence of a 25nt spike-in unique barcode in the positions 16 to 41 of the read. Using read 2 and the same sliding window strategy, adenosine region length was quantified starting at position 39 of the read.

Pooled RNAseq library preparation:

First, poly(A)+ RNA was isolated from 1µg of total RNA of up to 12 samples by two rounds of purification using Dynabeads mRNA DIRECT Kit (Invitrogen), according to the manufacturer's protocol. RNA fragmentation to ~150 nt fragment size was performed with the Invitrogen™ RNA Fragmentation Reagents kit (Invitrogen) according to the protocol. After every step, apart from those in which the sample was eluted in H2O, a cleanup with Dynabeads® MyOne™ Silane was performed according to the protocol. For the subsequent DNAse and dephosphorylation treatment, each sample
was incubated in T4 PNK (NEB T4 Polynucleotide Kinase), TURBO™ DNase and FastAP (Thermo Scientific™ FastAP Thermosensitive Alkaline Phosphatase) for 30 min in 37c in 5x FNKBuffer (1:1:2

ratio of T4 PNK-buffer : FastAP-buffer : H2O). 3' RNA barcode adapter ligation was performed with 20 pmol of RNA ILL adapter (**Table 3**) and 36 U T4 RNA ligase 1 for 1.5 h at room temperature for each sample. From this point onwards library preparation was performed like the mPAT-seq protocol.

For ribosomal depleted samples poly(A) selection step was omitted and following the 3' ligation of barcoded RNA adapters, all samples were pooled for ribosomal depletion with Ribo-Zero Gold rRNA Removal Kit (Yeast) (Illumina, MRZY1324) according to the kit protocol. All other steps of library preparation were performed identically.

Pooled RNAseq analysis:

Similarly to mPAT-seq, libraries were demultiplexed into individual samples, paired-end reads were aligned to the SacCer3 genome with identical parameters. Each read gene assignment was done with the intersect function from bedtools. TMM normalization and RPKM calculation was performed using the EdgeR package [65].

Transcript length estimation:

Yeast transcript length was calculated from the Nagalakshmi et al 3'UTR, 5'UTR, and ORF length annotation [66]. For the 3T3 and Hela cell lines annotations provided in Subtelny et al were used [30].

Principal component analysis (PCA):

For PCA analysis, vegetative growth and meiotic timecourse mean poly(A) tail per genes were scaled and then analysed using the R function *prcomp*. PC1 loadings per gene were used for subsequent analyses.

Gene ontology (GO) terms analysis:

For GO terms analysis, genes were ranked based on PC1 loadings obtained from the PCA analysis. This list was submitted to the FatScan tool of the Babelomics software [67] to detect overrepresented groups of genes where the tail is getting elongated or shortened across meiosis. GO terms with more than 200 members were filtered. GOs with a logarithm odds ratio above 50 (Elongated) or below -50 (Shortened) were selected and sorted based on the p-value.

Model for poly(A) tail length calculation:

The model of poly(A) tail calculation is a system of differential equations:

$$\frac{dNAmax}{dt} = \alpha - \beta N_{Amax}$$

$$\frac{dNA}{dt} = \beta N_{A+1} - \beta N_A \quad \text{For A} \neq A_{max}, A_{min}$$

$$\frac{dNAmin}{dt} = \beta N_{Amin+1} - \gamma N_{Amin}$$

Where α is production rate, β deadenylation rate and γ degradation rate. While A_{max} represents the length at which the molecules are formed, A_{min} represents the length at which the molecules are removed.

At steady state: $\frac{d}{dt} = 0$

$$N_{A+1} = N_A = N$$

$$N_{Amax} = \frac{\alpha}{\beta} = N$$

$$N_{Amin} = \frac{\beta}{\gamma} N_{Amin+1} = \frac{\beta}{\gamma} N = \frac{\alpha}{\gamma}$$

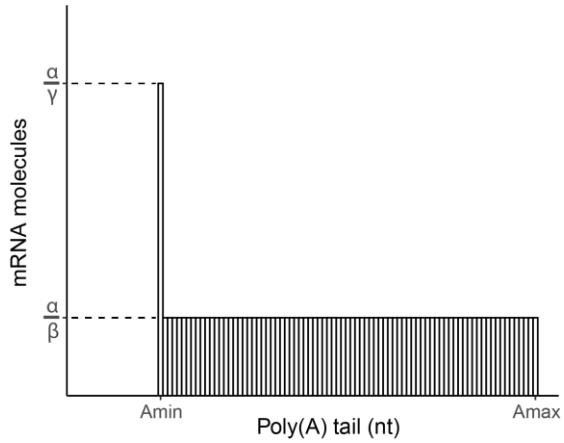

This implies that for a single transcript the distribution of tails will be determined by those parameters.

The total number of transcripts is defined as:

$$N_t = \sum_{A=A_{min}}^{A_{max}} N_A \qquad N_t = \frac{\alpha}{\gamma} + S\frac{\alpha}{\beta}$$

Where S is the number of deadenylation steps $S = A_{max} - A_{min}$

To calculate mean poly(A) tail length per gene:

$$L_{tail} = \frac{Amin \cdot \frac{\alpha}{\gamma} + S\frac{\alpha}{\beta}(Amin + \frac{S+1}{2})}{\frac{\alpha}{\gamma} + S\frac{\alpha}{\beta}} = \frac{\frac{\alpha}{\gamma\beta}(\beta A_{min} + S\gamma A_{min} + S\gamma\frac{S+1}{2})}{\beta + S\gamma} = \frac{\frac{\beta}{\gamma}A_{min} + S(A_{min} + \frac{S+1}{2})}{\frac{\beta}{\gamma} + S}$$

$$= A_{min}\frac{\frac{\beta}{\gamma} + S(1 + \frac{S+1}{2A_{min}})}{\frac{\beta}{\gamma} + S}$$

Data availability:

The data sets generated in this study for analyzing poly(A) tail length and RNA expression are available on GEO under the accession number GSE171329. Tail-seq and PAL-seq data were obtained from: Gene Expression Omnibus (GEO) database (accession numbers GSE116355 and GSE134660).

Code availability:

Code for the analyses described in this paper is available from the corresponding author upon request.

Table 1 Yeast Strains

S. cerevisiae SK1 WT (SAy821) MAT a/α	Sudeep D. Agarwala [28]
S. cerevisiae SK1 ccr4Δ/Δ MAT a/α Ccr4::KanMX6 /Ccr4::natMX	This study.
S. cerevisiae SK1 pop2Δ/Δ MAT a/α Pop2::KanMX6 /Pop2::natMX	This study.
S. cerevisiae SK1 xrn1Δ/Δ MAT a/α l Xrn1::KanMX6 /Xrn1::hphMX	This study.
S. cerevisiae SK1 pCup1-Ccr4 MAT a/α NAT::pCup1::Ccr4	This study.
S. cerevisiae SK1 Xrn1-GFP MAT a/α Xrn1::GFP::KanMX6	This study.
S. cerevisiae SK1 a/a MATa	Folkert van Werven [35]
S. cerevisiae SK1 degron-Xrn1 MATa/α (pCUP1-TIR1) XRN1-3V5-IAA7:KanMX6	Folkert van Werven

Table 2 Poly(A) tail DNA spike-ins

Spike-in	Sequence
11A	AGA CGT GTG CTC TTC CGA TCT NNN NNN NNN NNN NNN TGC TTT TTT TTT TTG AGC TTC AAT AGG TAT AAC TCC GCA AGA TCG GAA GAG CGT CGT GTA
23A	AGA CGT GTG CTC TTC CGA TCT NNN NNN NNN NNN NNN TGC TTT TTT TTT TTT TTT TTT TTT CTG ATT ATC AAA CAG GAG ATA TAA TAG ATC GGA AGA GCG TCG TGT A
31A	AGA CGT GTG CTC TTC CGA TCT NNN NNN NNN NNN NNN TGC TTT TTT TTT TTT TTT TTT TTT TTT TTT TAG CCG TAT GTG GGA CGA CTT CGT CCA GAT CGG AAG AGC GTC GTG TA
51A	AGA CGT GTG CTC TTC CGA TCT NNN NNN NNN NNN NNN TGC TTT TTT TTT TTT TTT TTT TTT TTT TTT TTT TTT TTT TTT TTT TTT CAC GAC CTA GGG CCC CAG CTG GCG CAG ATC GGA AGA GCG TCG TGT A
76A	AGA CGT GTG CTC TTC CGA TCT NNN NNN NNN NNN NNN TGC TTT TTT TTT TTT TTT TTT TTT TTT TTT TTT TTT TTT TTT TTT TTT TTT TTT TTT TTT TTT TTT TTT TTT TTT TTT TTT TTT TTT TTT TTT TTT TTT TAA CAA GCT GAG GAT CGC AAT CCT TTA GAT CGG AAG AGC GTC GTG TA

Table 3 Primers and oligos.

Oligo	Sequence
rTd RT primer	AGACGTGTGCTCTTCCG
5iLL-22 adapter	5'-/5Phos/AGATCGGAAGAGCGTCGTGTAG/3ddC/ -3'
RNA ILL	/5Phos/7ntUniqueBarcode/NNNAGATCGGAAGAGCACACGTCT/3SpC3/
qCCR4-forward	AATAGCCTCACGGAACTGCC
qCCR4-reverse	AGCCTAGTTCCGCTGGTAGA
qACT1-forward	GCCGGTGACGACGCTCCT
qACT1-reverse	CCTTGGTGTCTTGGTCTACCGA

Supplementary Note 1:

Poly (A) model is robust to fuzziness in A_{min} and A_{max}:

To evaluate the robustness of our model we relaxed the assumptions regarding fixed A_{min} and A_{max} values across different genes. We simulated poly(A) tail distributions when A_{min} and A_{max} distribution is not fixed but instead varies between genes, on the basis of a normal distribution with increasing standard deviation. For simplicity, in these simulations, we kept deadenylation and deadenylation rate constant for all the genes, but the conclusions are identical if we allow variability in these parameters between different genes. Importantly, increased variability in A_{min} and A_{max} gave rise to increasingly 'long-tailed' distributions of poly(A) tail length **(Fig. S4A-B)**, mirroring the actual data. However, the correlation between the short fraction of tails and mean poly(A) tail length is robust to these changes **(Fig. S4C)**.

Alternative model for poly(A) tail length calculation where deadenylation rate is a function of tail length:

The model of poly(A) tail calculation is a system of differential equations:

$$\frac{dNAmax}{dt} = \alpha - \beta_{Amax} N_{Amax}$$

$$\frac{dNA}{dt} = \beta_{A+1} N_{A+1} - \beta_A N_A \quad \text{For A} \neq A_{max}, A_{min}$$

$$\frac{dNAmin}{dt} = \beta_{Amin+1} N_{Amin+1} - \gamma N_{Amin}$$

Where α is production rate, γ degradation rate, and β deadenylation rate which is a function of tail length. While A_{max} represents the length at which the molecules are formed, A_{min} represents the length at which the molecules are removed.

At steady state: $\frac{d}{dt} = 0$

$$N_{Amax} = \frac{\alpha}{\beta_{Amax}} = N$$

$$N_A = \frac{\beta_{A+1}}{\beta_A} N_{A+1} \qquad N_A \beta_A = \Omega = \alpha$$

$$N_{Amin} = \frac{\beta_{Amin}}{\gamma} N_{Amin+1} = \frac{\beta}{\gamma} N = \frac{\alpha}{\gamma}$$

This implies that for a single transcript the distribution of tails will be determined by those parameters.

The total number of transcripts is defined as:

$$N_t = \sum_{A=A_{min}}^{A_{max}} N_A \qquad N_t = \frac{\alpha}{\gamma} + S\frac{\alpha}{<\beta>}$$

Where S is the number of deadenylation steps and $< \beta >$is the average deadenylation rate defined as:
$$\frac{1}{<\beta>} = \frac{1}{S}\sum_{A=A_{min}+1}^{A_{max}} \frac{1}{\beta_A}$$

We defined the relationship between $\beta$and A_{length} either linear or exponential :

Linear: $\beta = \frac{1}{a-bA}$

Exponential: $\beta = ae^{bA}$

Where a and $b$are constants that define the strength of deadenylation and the strength of the impact of tail length in deadenylation respectively.

In the case of a linear model, we observed that long-tailed distribution of poly(A) tails (as are observed in our data) can be achieved exclusively under scenarios in which degradation rate is a positive function of tail length, but not when it is a negative function **(Fig. S4D)**. Similar results are observed when the relationship between poly(A) tail length and deadenylation rate is exponential **(Fig. S4E)**. Importantly, also under these scenarios the relationship between tail length and the deadenylation/degradation rate are maintained **(Fig. S4D-E)**.

We conclude that the deviation of the experimental data from the model could be attributed in part to fuzziness in Amin and Amax distributions, or potentially also to specific scenarios involving some dependency between tail length and deadenylation rates. In both cases, it is possible to capture such effects via slight modulations of our model, and in both cases such modulations maintain the fundamental relationship between deadenylation/degradation ratio and tail length, and therefore would not be expected to affect the main conclusions of the work.

References:

1. Lingner, J., Kellermann, J. & Keller, W. Cloning and expression of the essential gene for poly(A) polymerase from S. cerevisiae. *Nature* vol. 354 496–498 (1991).
2. Tucker, M., Staples, R. R., Valencia-Sanchez, M. A., Muhlrad, D. & Parker, R. Ccr4p is the catalytic subunit of a Ccr4p/Pop2p/Notp mRNA deadenylase complex in Saccharomyces cerevisiae. *EMBO J.* **21**, 1427–1436 (2002).
3. LaGrandeur, T. E. & Parker, R. Isolation and characterization of Dcp1p, the yeast mRNA decapping enzyme. *EMBO J.* **17**, 1487–1496 (1998).
4. Hsu, C. L. & Stevens, A. Yeast cells lacking 5'-->3' exoribonuclease 1 contain mRNA species that are poly(A) deficient and partially lack the 5' cap structure. *Mol. Cell. Biol.* **13**, 4826–4835 (1993).
5. Muhlrad, D., Decker, C. J. & Parker, R. Deadenylation of the unstable mRNA encoded by the yeast MFA2 gene leads to decapping followed by 5'-->3' digestion of the transcript. *Genes Dev.* **8**, 855–866 (1994).
6. Larimer, F. W. & Stevens, A. Disruption of the gene XRN1, coding for a 5'----3' exoribonuclease, restricts yeast cell growth. *Gene* **95**, 85–90 (1990).
7. Hsu, C. L. & Stevens, A. Yeast cells lacking 5'--> 3'exoribonuclease 1 contain mRNA species that are poly (A) deficient and partially lack the 5'cap structure. *Mol. Cell. Biol.* (1993).
8. Goldstrohm, A. C. & Wickens, M. Multifunctional deadenylase complexes diversify mRNA control. *Nat. Rev. Mol. Cell Biol.* **9**, 337–344 (2008).
9. Eisen, T. J. *et al.* The Dynamics of Cytoplasmic mRNA Metabolism. *Mol. Cell* **77**, 786–799.e10 (2020).
10. Brown, C. E. & Sachs, A. B. Poly(A) tail length control in Saccharomyces cerevisiae occurs by message-specific deadenylation. *Mol. Cell. Biol.* **18**, 6548–6559 (1998).
11. Goldstrohm, A. C., Hook, B. A., Seay, D. J. & Wickens, M. PUF proteins bind Pop2p to regulate messenger RNAs. *Nat. Struct. Mol. Biol.* **13**, 533–539 (2006).
12. Goldstrohm, A. C., Seay, D. J., Hook, B. A. & Wickens, M. PUF protein-mediated deadenylation is catalyzed by Ccr4p. *J. Biol. Chem.* **282**, 109–114 (2007).
13. Webster, M. W., Stowell, J. A. & Passmore, L. A. RNA-binding proteins distinguish between similar sequence motifs to promote targeted deadenylation by Ccr4-Not. *Elife* **8**, (2019).
14. Du, H. *et al.* YTHDF2 destabilizes m6A-containing RNA through direct recruitment of the CCR4–

NOT deadenylase complex. *Nat. Commun.* **7**, 12626 (2016).

15. Fabian, M. R. *et al.* miRNA-mediated deadenylation is orchestrated by GW182 through two conserved motifs that interact with CCR4–NOT. *Nat. Struct. Mol. Biol.* **18**, 1211 (2011).
16. Chekulaeva, M. *et al.* miRNA repression involves GW182-mediated recruitment of CCR4–NOT through conserved W-containing motifs. *Nat. Struct. Mol. Biol.* **18**, 1218 (2011).
17. Lim, J., Lee, M., Son, A., Chang, H. & Kim, V. N. MTAIL-seq reveals dynamic poly(A) tail regulation in oocyte-to-embryo development. *Genes and Development* **30**, 1671–1682 (2016).
18. Eichhorn, S. W. *et al.* mRNA poly(A)-tail changes specified by deadenylation broadly reshape translation in Drosophila oocytes and early embryos. *eLife* vol. 5 (2016).
19. Kojima, S., Sher-Chen, E. L. & Green, C. B. Circadian control of mRNA polyadenylation dynamics regulates rhythmic protein expression. *Genes Dev.* **26**, 2724–2736 (2012).
20. Yao, X., Kojima, S. & Chen, J. Critical role of deadenylation in regulating poly(A) rhythms and circadian gene expression. *PLoS Comput. Biol.* **16**, e1007842 (2020).
21. Chen, C.-Y. A., Zhang, Y., Xiang, Y., Han, L. & Shyu, A.-B. Antagonistic actions of two human Pan3 isoforms on global mRNA turnover. *RNA* **23**, 1404–1418 (2017).
22. Chen, C.-Y. A., Strouz, K., Huang, K.-L. & Shyu, A.-B. Tob2 phosphorylation regulates global mRNA turnover to reshape transcriptome and impact cell proliferation. *RNA* **26**, 1143–1159 (2020).
23. Yi, H. *et al.* PABP Cooperates with the CCR4-NOT Complex to Promote mRNA Deadenylation and Block Precocious Decay. *Mol. Cell* **70**, 1081–1088.e5 (2018).
24. Chu, S. The Transcriptional Program of Sporulation in Budding Yeast TL - 282. *Science* **282 VN -** , 699–706 (1998).
25. Brar, G. A. *et al.* High-resolution view of the yeast meiotic program revealed by ribosome profiling. *Science* **335**, 552–557 (2012).
26. Cheng, Z. *et al.* Pervasive, Coordinated Protein-Level Changes Driven by Transcript Isoform Switching during Meiosis. *Cell* **172**, 910–923.e16 (2018).
27. Lardenois, A. *et al.* Execution of the meiotic noncoding RNA expression program and the onset of gametogenesis in yeast require the conserved exosome subunit Rrp6. *Proc. Natl. Acad. Sci. U. S. A.* **108**, 1058–1063 (2011).
28. Agarwala, S. D., Blitzblau, H. G., Hochwagen, A. & Fink, G. R. RNA methylation by the MIS

complex regulates a cell fate decision in yeast. *PLoS Genet.* **8**, 1–13 (2012).

29. Schwartz, S. *et al.* High-resolution mapping reveals a conserved, widespread, dynamic mRNA methylation program in yeast meiosis. *Cell* **155**, 1409–1421 (2013).
30. Subtelny, A. O., Eichhorn, S. W., Chen, G. R., Sive, H. & Bartel, D. P. Poly(A)-tail profiling reveals an embryonic switch in translational control. *Nature* **508**, 66–71 (2014).
31. Chang, H., Lim, J., Ha, M. & Kim, V. N. TAIL-seq: genome-wide determination of poly(A) tail length and 3' end modifications. *Mol. Cell* **53**, 1044–1052 (2014).
32. Legnini, I., Alles, J., Karaiskos, N., Ayoub, S. & Rajewsky, N. FLAM-seq: full-length mRNA sequencing reveals principles of poly(A) tail length control. *Nat. Methods* **16**, 879–886 (2019).
33. Mattijssen, S., Iben, J. R., Li, T., Coon, S. L. & Maraia, R. J. Single molecule poly(A) tail-seq shows LARP4 opposes deadenylation throughout mRNA lifespan with most impact on short tails. *Elife* **9**, (2020).
34. Ripley, B. & Others. MASS: support functions and datasets for Venables and Ripley's MASS. *R package version* **7**, 3–29 (2011).
35. van Werven, F. J. *et al.* Transcription of two long noncoding RNAs mediates mating-type control of gametogenesis in budding yeast. *Cell* **150**, 1170–1181 (2012).
36. Simchen, G., Piñon, R. & Salts, Y. Sporulation in Saccharomyces cerevisiae: premeiotic DNA synthesis, readiness and commitment. *Exp. Cell Res.* **75**, 207–218 (1972).
37. Parker, R. RNA degradation in Saccharomyces cerevisae. *Genetics* **191**, 671–702 (2012).
38. Nishimura, K., Fukagawa, T., Takisawa, H., Kakimoto, T. & Kanemaki, M. An auxin-based degron system for the rapid depletion of proteins in nonplant cells. *Nat. Methods* **6**, 917–922 (2009).
39. Morris, J. Z., Hong, A., Lilly, M. A. & Lehmann, R. twin, a CCR4 homolog, regulates cyclin poly(A) tail length to permit Drosophila oogenesis. *Development* **132**, 1165–1174 (2005).
40. Molin, L. & Puisieux, A. C. elegans homologue of the Caf1 gene, which encodes a subunit of the CCR4-NOT complex, is essential for embryonic and larval development and for meiotic progression. *Gene* **358**, 73–81 (2005).
41. Berthet, C. *et al.* CCR4-associated factor CAF1 is an essential factor for spermatogenesis. *Mol. Cell. Biol.* **24**, 5808–5820 (2004).
42. Etcheverry, T. Induced expression using yeast copper metallothionein promoter. *Methods Enzymol.* **185**, 319–329 (1990).

43. Lima, S. A. *et al.* Short poly(A) tails are a conserved feature of highly expressed genes. *Nature Structural & Molecular Biology* vol. 24 1057–1063 (2017).
44. Sheth, U. & Parker, R. Decapping and decay of messenger RNA occur in cytoplasmic processing bodies. *Science* **300**, 805–808 (2003).
45. Grousl, T., Opekarová, M., Stradalova, V., Hasek, J. & Malinsky, J. Evolutionarily Conserved 5'-3' Exoribonuclease Xrn1 Accumulates at Plasma Membrane-Associated Eisosomes in Post-Diauxic Yeast. *PLOS ONE* vol. 10 e0122770 (2015).
46. Zhang, B., Butler, A. M., Shi, Q., Xing, S. & Herman, P. K. P-Body Localization of the Hrr25/Casein Kinase 1 Protein Kinase Is Required for the Completion of Meiosis. *Mol. Cell. Biol.* **38**, (2018).
47. Lim, J. *et al.* Uridylation by TUT4 and TUT7 marks mRNA for degradation. *Cell* **159**, 1365–1376 (2014).
48. Gillian-Daniel, D. L., Gray, N. K., Aström, J., Barkoff, A. & Wickens, M. Modifications of the 5' cap of mRNAs during Xenopus oocyte maturation: independence from changes in poly(A) length and impact on translation. *Mol. Cell. Biol.* **18**, 6152–6163 (1998).
49. Zhao, H. *et al.* A Role for the Respiratory Chain in Regulating Meiosis Initiation in Saccharomyces cerevisiae. *Genetics* **208**, 1181–1194 (2018).
50. Jambhekar, A. & Amon, A. Control of meiosis by respiration. *Curr. Biol.* **18**, 969–975 (2008).
51. Weidberg, H., Moretto, F., Spedale, G., Amon, A. & van Werven, F. J. Nutrient Control of Yeast Gametogenesis Is Mediated by TORC1, PKA and Energy Availability. *PLoS Genet.* **12**, e1006075 (2016).
52. Kim, J. H. & Richter, J. D. Opposing polymerase-deadenylase activities regulate cytoplasmic polyadenylation. *Mol. Cell* **24**, 173–183 (2006).
53. Lim, J. *et al.* Mixed tailing by TENT4A and TENT4B shields mRNA from rapid deadenylation. *Science* **361**, 701–704 (2018).
54. Yamashita, A. *et al.* Concerted action of poly(A) nucleases and decapping enzyme in mammalian mRNA turnover. *Nat. Struct. Mol. Biol.* **12**, 1054–1063 (2005).
55. Shalem, O., Groisman, B., Choder, M., Dahan, O. & Pilpel, Y. Transcriptome kinetics is governed by a genome-wide coupling of mRNA production and degradation: a role for RNA Pol II. *PLoS Genet.* **7**, e1002273 (2011).

56. Slobodin, B. *et al.* Transcription Dynamics Regulate Poly(A) Tails and Expression of the RNA Degradation Machinery to Balance mRNA Levels. *Molecular Cell* vol. 78 434–444.e5 (2020).
57. Amrani, N., Ghosh, S., Mangus, D. A. & Jacobson, A. Translation factors promote the formation of two states of the closed-loop mRNP. *Nature* **453**, 1276–1280 (2008).
58. Eisen, T. J., Eichhorn, S. W., Subtelny, A. O. & Bartel, D. P. MicroRNAs Cause Accelerated Decay of Short-Tailed Target mRNAs. *Mol. Cell* **77**, 775–785.e8 (2020).
59. Chang, C.-T. *et al.* A low-complexity region in human XRN1 directly recruits deadenylation and decapping factors in 5'-3' messenger RNA decay. *Nucleic Acids Res.* **47**, 9282–9295 (2019).
60. Haas, G. *et al.* HPat provides a link between deadenylation and decapping in metazoa. *J. Cell Biol.* **189**, 289–302 (2010).
61. Ozgur, S., Chekulaeva, M. & Stoecklin, G. Human Pat1b connects deadenylation with mRNA decapping and controls the assembly of processing bodies. *Mol. Cell. Biol.* **30**, 4308–4323 (2010).
62. Perea-García, A., Miró, P., Jiménez-Lorenzo, R., Martínez-Pastor, M. T. & Puig, S. Sequential recruitment of the mRNA decay machinery to the iron-regulated protein Cth2 in Saccharomyces cerevisiae. *Biochim. Biophys. Acta Gene Regul. Mech.* **1863**, 194595 (2020).
63. Dobin, A. *et al.* STAR: ultrafast universal RNA-seq aligner. *Bioinformatics* vol. 29 15–21 (2013).
64. Quinlan, A. R. & Hall, I. M. BEDTools: a flexible suite of utilities for comparing genomic features. *Bioinformatics* **26**, 841–842 (2010).
65. Robinson, M. D., McCarthy, D. J. & Smyth, G. K. edgeR: a Bioconductor package for differential expression analysis of digital gene expression data. *Bioinformatics* **26**, 139–140 (2010).
66. Nagalakshmi, U. *et al.* The transcriptional landscape of the yeast genome defined by RNA sequencing. *Science* **320**, 1344–1349 (2008).
67. Al-Shahrour, F., Minguez, P., Vaquerizas, J. M., Conde, L. & Dopazo, J. BABELOMICS: a suite of web tools for functional annotation and analysis of groups of genes in high-throughput experiments. *Nucleic Acids Res.* **33**, W460–4 (2005).
68. Institute, B. Picard tools. (2016).